Evaluating Simplifications of Subsurface Process Representations for Field-scale Permafrost Hydrology Models

Bo Gao, Ethan T. Coon

Environmental Sciences Division, Oak Ridge National Laboratory, Oak Ridge, Tennessee, USA

Correspondence to: Ethan T. Coon (coonet@ornl.gov)

Abstract. Permafrost degradation within a warming climate poses a significant environmental threat through both the permafrost carbon feedback and damage to human communities and infrastructure. Understanding this threat relies on better understanding and numerical representation of thermo-hydrological permafrost processes, and the subsequent accurate prediction of permafrost dynamics. All models include simplified assumptions, implying a tradeoff between model complexity and prediction accuracy. The main purpose of this work is to investigate this tradeoff when applying the following commonly made assumptions: (1) assuming equal density of ice and liquid water in frozen soil; (2) neglecting the effect of cryosuction in unsaturated freezing soil; and (3) neglecting advective heat transport during soil freezing and thaw. This study designed a set of 62 numerical experiments using the Advanced Terrestrial Simulator (ATS v1.2) to evaluate the effects of these choices on permafrost hydrological outputs, including both integrated and pointwise quantities. Simulations were conducted under different climate conditions and soil properties from three different sites in both column- and hillslope-scale configurations. Results showed that amongst the three physical assumptions, soil cryosuction is the most crucial yet commonly ignored process. Neglecting cryosuction, on average, can cause 10% ~ 20% error in predicting evaporation, 50% ~ 60% error in discharge, 10% ~ 30% error in thaw depth, and 10% ~ 30% error in soil temperature at 1 m beneath surface. The prediction error for subsurface temperature and water saturation is more obvious at hillslope scales due to the presence of lateral flux. By comparison, using equal ice-liquid density has a minor impact on most hydrological metrics of interest, but significantly affects soil water saturation with an averaged 5% ~ 15% error. Neglecting advective heat transport presents the least error, 5% or even much lower, in most metrics of interest for a large-scale Arctic tundra system without apparent influence caused by localized groundwater flow, and can decrease the simulation time at hillslope scales by 40% ~ 80%. By challenging these commonly made assumptions, this work provides permafrost

hydrology scientists important context for understanding the underlying physical processes, including allowing modelers to better choose the appropriate process representation for a given modeling experiment.

1 Introduction

Permafrost describes a state of ground which stays frozen continuously over multiple years, which may cover an entire region (e.g., Arctic tundra) or occur in isolation (e.g., alpine top). From the perspective of scope, permafrost occupies approximately 23.9% (22.79 million km^2) of the exposed land area of the northern hemisphere (Zhang et al., 2008), as well as alpine regions and Antarctica in the southern hemisphere. Permafrost areas store a vast amount of organic carbon, of which most is stored in perennially frozen soils (Hugelius et al., 2014). If the organic carbon is exposed due to permafrost thaw, it is likely to decay with microbial activity, releasing greenhouse gas to the atmosphere and exacerbating global warming. In Arctic tundra, permafrost also plays an important role in maintaining water, habitat of wildlife, landscape, and infrastructure (Berteaux et al., 2017; Dearborn et al., 2021; Hjort et al., 2018; Sugimoto et al., 2002). Permafrost degradation may cause significant damage to the local ecosystem, reshape the surface and subsurface hydrology, and eventually influence the global biosphere (Cheng and Wu, 2007; Jorgenson et al., 2001; Tesi et al., 2016; Walvoord and Kurylyk, 2016). Therefore, the occurrent and potential impacts motivate the development of computational models with the goal of better understanding the thermal and hydrological processes in permafrost regions, and consequently to predict permafrost thaw more accurately.

Simulating soil freezing and thaw processes is a challenging task that incorporates mass and energy

60 transfer among atmosphere, snowpack, land surface (perhaps with free water), and a variably
61 saturated subsurface. Several hydrological models with different complexity and applicable scales
62 have been developed to investigate the complicated interactions. Reviews of permafrost models
63 based on empirical and physical representations using analytical and numerical solutions can be
64 found in (Bui et al., 2020; Dall'Amico et al., 2011; Grenier et al., 2018; Jan et al., 2020; Kurylyk
65 et al., 2014; Kurylyk and Watanabe, 2013; Riseborough et al., 2008). Process-rich models which
66 aim to predict permafrost change through direct simulation of mass and energy transport, such as
67 the Advanced Terrestrial Simulator (ATS; Painter et al., 2016), GEOtop (Endrizzi et al., 2014),
68 CryoGrid 3 (Westermann et al., 2016), PFLOTRAN-ICE (Karra et al., 2014), and SUTRA-ICE
69 (McKenzie et al., 2007), have been demonstrated to describe thermal permafrost hydrology under
70 various climate conditions. Nominally, representing more physical process complexity should
71 improve predictions of permafrost change, but the degree to which each process affects metrics of
72 permafrost hydrology is highly uncertain and likely differs by scale. Philosophically, models
73 provide a useful tool precisely because they allow counterfactual experiments where processes are
74 simplified to understand the relative importance of that process; thus, challenging assumptions
75 about process simplifications are a significant part of both general process understanding,
76 benefiting the permafrost hydrology community writ large, and model representations, benefiting
77 the community of model developers and users.
78 Even in the most process-rich models of permafrost change, three such physical simplifications
79 are often made: representing water at constant density (thereby neglecting the expansion of ice
80 relative to liquid water), neglecting cryosuction of water in unsaturated, partially frozen soils, and
81 neglecting advective heat transport.
82 First, because of the lower density of ice than liquid water, freezing water must expand the volume
83 of the porous media, push liquid water into nearby volume, or otherwise expand the volume
84 occupied by that water. As most of the current set of models operate under the assumption of a
85 rigid solid matrix and thus the absence of mechanical equations describing matrix deformation or
86 frost heave, including this expansion typically results in large pressures that must be offset by grain
87 compressibility or another mechanism. Therefore, the densities of ice and liquid water are
88 frequently assumed equal (e.g., Dall'Amico et al., 2011; Devoie and Craig, 2020; Weismüller et
89 al., 2011). It is uncertain whether this simplification affects predictions of permafrost change and
90 thermal hydrology.

91   Second, cryosuction describes the redistribution of water in partially frozen, unsaturated soils
92   caused by increased matric suction. At the interface of ice and liquid water, negative pressures
93   result in the migration of liquid water toward the freezing front and the subsequent increase of ice
94   content. Several approaches representing cryosuction in models are used (Dall'Amico et al., 2011;
95   Noh et al., 2012; Painter and Karra, 2014; Stuurop et al., 2021), either in an empirical form or
96   physically derived from the generalized Clapeyron equation. Other process-rich models have
97   ignored cryosuction entirely (McKenzie et al., 2007; Viterbo et al., 1999). Dall'Amico et al. (2011),
98   Painter (2011) and Painter and Karra (2014) evaluated their respective Clapeyron equation based
99   cryosuction models in soil column freezing simulations and presented a good match between
100   simulations and laboratory experiments in total water content (liquid and ice). Recently, Stuurop
101   et al. (2021) applied an empirical expression, a physics-based expression, and no cryosuction in
102   simulating soil column freezing process. They compared the simulated results with observations
103   from laboratory experiments. This comparison demonstrated minor differences between empirical
104   and Clapeyron-based cryosuction expressions, but the simulation without cryosuction cannot
105   predict the distribution of total water content in a laboratory-scale soil column. To our knowledge,
106   there is still no literature showing the effect of cryosuction on plot-scale permafrost predictions.
107   Third, heat transport in process-rich models is described using an energy conservation equation,
108   mainly including heat conduction, latent heat exchange, and heat advection. From a continuum-
109   scale perspective, conductive heat transport is expressed in the form of a diffusive term based
110   on Fourier's law. Latent heat exchange accompanies phase change which alters the system enthalpy.
111   Advective heat transport describes the energy exchange caused by the flow of liquid water driven
112   by a hydraulic gradient (i.e., forced convection), which is expressed through an advective term in
113   energy balance equations. Additionally, other mechanisms that control heat transport, such as
114   water vapor movement, thermal dispersion, etc., are neglected by nearly all models of permafrost
115   and are not considered here. Several studies have demonstrated the importance of advective heat
116   transport in permafrost hydrology through field observation analysis or modeling comparison.
117   Such situations where advective heat transport makes important contributions roughly fall into
118   three categories. The first centers on the development of taliks beneath lakes, ponds, topographic
119   depressions, or other discontinuous permafrost effects (e.g., Dagenais et al., 2020; Liu et al., 2022;
120   Luethi et al., 2017; McKenzie and Voss, 2013; Rowland et al., 2011). The second focuses on
121   microtopographic features that focus significant amount of water through small areas. This

122 includes both low-center ice wedge polygons associated with the formation of thermokarst ponds

123 (e.g., Abolt et al., 2020; Harp et al., 2021) and thermo-erosion gullies (e.g., Fortier et al., 2007;

124 Godin et al., 2014). In these cases, large, focused flows across small spatial scales allow advective

125 heat transport to dominate. The last category includes those studying the construction and

126 maintenance of infrastructure influenced by groundwater flow (e.g., Chen et al., 2020). Thus, these

127 studies focus on either location-specific or scale-limited problems. As McKenzie and Voss (2013)

128 stated, whether heat advection outweighs heat conduction depends on soil permeability,

129 topography, and groundwater availability. Relative to these special cases at small scales, we are

130 more interested in to what extent advective heat transport associated with liquid water flow

131 contributes to permafrost hydrologic change in a hillslope-scale or larger Arctic system. The Arctic

132 systems, discussed hereinafter in this paper, refer to those with negligible influence caused by

133 localized groundwater flow features as the three categories mentioned above.

134 To clarify the significant differences in model representations of permafrost, we investigate the

135 influence of including or not including these processes on permafrost change at plot-to-hillslope

136 scales. For ice density, we compare simulations with and without differences in ice density relative

137 to water density; for cryosuction, we compare simulations using a Clapyron equation-based

138 expression and excluding the cryosuction effect; and for heat transport, we compare simulations

139 including or neglecting advective heat transport. All comparisons are carried out across a range of

140 Arctic climate conditions and soil properties from three different sites. Both 1D soil-column-scale

141 and 2D hillslope-scale models are considered, in which varying hillslope geometries (i.e.,

142 convergent/divergent hillslope) and aspects (i.e., north/south) are included. The aim of this study

143 is to provide better understanding of physical processes to permafrost hydrologists in general; and

144 to offer some concrete insights to the model users and developers working on the process-rich

145 models with similar theories and equation basis.

146 **2 Theory**

147 The Advanced Terrestrial Simulator (ATS v1.2) (Coon et al., 2020) configured in permafrost mode

148 (Jan et al., 2018, 2020; Painter et al., 2016) was used to implement all numerical experiments in

149 this study. ATS is a process-rich code developed for simulating integrated surface and subsurface

150 hydrological processes, specifically capable of permafrost applications. It has been shown to

151 successfully compare to observations of seasonal soil freezing and thaw processes at different

152 scales. This includes 1D models of vertical energy transport typical of large-scale flatter regions

153 (Atchley et al., 2015), and 2D models admitting lateral flow and transport in Arctic fens (Sjöberg

154 et al., 2016), and polygonal ground (Jan et al., 2020).

155 The permafrost configuration of ATS comprises coupled water flow and energy transfer within

156 variably saturated soils and at land surfaces, a surface energy balance model describing thermal

157 processes in snow, and a snow distribution module for surface microtopography (Painter et al.,

158 2016). The subsurface system solves a three-phase (liquid, ice, gas), two-component (water vapor,

159 air) Richards-type mass balance equation with Darcy's law and an advection-conduction energy

160 balance equation. The surface system includes an overland flow model with diffusion wave

161 approximation, and an energy balance equation with an introduced temperature-dependent factor

162 describing the effect of surface water freezing. The subsurface system and surface system are

163 coupled through the continuity of pressure, temperature, and the corresponding fluxes by

164 incorporating the surface equations as boundary conditions of the subsurface equations (Coon et

165 al., 2020). The evolution of a snowpack and its effect on the surface energy balance is described

166 using an energy balance approach based on a subgrid model concept that includes all major heat

167 fluxes at the land surface. For a more detailed description of the permafrost configuration and

168 implementation in ATS, as well as key mathematical equations, the reader is referred to Painter et

169 al. (2016). Changes in this "most complex" model of permafrost hydrology are enabled by the

170 Arcos multiphysics library leveraged in ATS; this allows the precise model physics to be specified

171 and configured at runtime through the use of a dependency graph describing swappable

172 components in the model physics (Coon et al., 2016).

2.1 Ice density

174 The density of ice (kg/m^3) is represented as a Taylor series expansion in both temperature and

175 pressure:

176 $$\rho_i = [a + (b + c\Delta T) \times \Delta T] \times (1 + \alpha \Delta p) \tag{1}$$

177 and the density of liquid water (kg/m^3) is represented as:

178 $$\rho_l = [a + (b + (c + d\Delta T) \times \Delta T) \times \Delta T] \times (1 + \alpha \Delta p) \tag{2}$$

179 where $\Delta T = T - 273.15$, $\Delta p = p_l - 1e5$, T and p_l are temperature (K) and liquid pressure (>101325

180 Pa), respectively; and a, b, c, d, α are constant coefficients, listed in Table 1. Under conditions of

181 equal density, we assume $\rho_i = \rho_l$.

Table 1 Coefficients in density of ice and liquid

	a	b	c	d	α
ρ_i	916.724	-0.147143	-2.38e-4	–	1.0e-10
ρ_l	999.915	0.0416516	-1.01e-2	2.06e-4	5.0e-10

2.2 Cryosuction

Several models are available in the literature describing the relationship between unfrozen water content and temperature or matric suction (e.g., Ren et al., 2017; Stuurop et al., 2021), which is also termed the soil freezing characteristic curve. These models are either associated with temperature empirically or related to the soil water retention curve through the Clapeyron equation. The latter approach normally incorporates the soil cryosuction process, while the former does not. Painter and Karra (2014) proposed a constitutive model which relates the soil unfrozen water content with the van Genuchten model (van Genuchten, 1980) based on the Clapeyron equation:

$$s_l = \begin{cases} S_*(-\beta \rho_l L_f \vartheta), \vartheta < \vartheta_f \\ S_*(p_g - p_l), \vartheta \geq \vartheta_f \end{cases}, \quad \vartheta = \frac{T(K)-273.15}{273.15}, \quad \vartheta_f = -\frac{\psi_*(1-s_g)}{\beta L_f \rho_l}$$
$$s_i = 1 - s_l/S_*(p_g - p_l) \tag{3}$$

where s_n is the saturation of n-phase and the subscripts $n = $ l, i, g are liquid, ice, and gas phases, respectively; β is a coefficient; L_f is the heat fusion of ice; p_n ($n = $ l, g) is the pressure of n-phase; S_* is the Van Genuchten model. This physically derived formulation can describe the change of matric suction in the frozen zone due to the change of ice content, and thus has the capacity to represent cryosuction.

Alternatively, the unfrozen water content can be also expressed as a single-variable function dependent on sub-freezing temperature for a given soil, ignoring the effect of cryosuction, such as the following (McKenzie et al., 2007):

$$s_l = s_r + (s_{sat} - s_r)\exp\left[-\left(\frac{T(K)-273.15}{\omega}\right)^2\right]$$
$$s_i = S_*(p_g - p_l) - s_l \tag{4}$$

where s_r, s_{sat} are saturations of liquid water at residual and saturated conditions, respectively; ω is a constant coefficient. In this case, the van Genuchten model was used to determine the total water content, including liquid water and ice.

2.3 Advective heat transport

The energy conservation equation of the subsurface system is given by:

206 $\quad\frac{\partial}{\partial t}\left[\phi\sum_{n=\text{l,i,g}}(\rho_n s_n u_n) + (1-\phi)c_{\text{v,soil}}T\right] + \underbrace{\nabla\cdot(\rho_l h_l \mathbf{V_l})}_{\text{advective heat}} \underbrace{-\nabla\cdot(\kappa_e\nabla T)}_{\text{conductive heat}} = Q_E$ $\qquad$ (5)

207 where ϕ is porosity; u_n is the specific internal energy of phase ($n \in \{\text{l, i, g}\}$); $c_{\text{v,soil}}$ (J m^{-3} K^{-1}) is

208 the volumetric heat capacity of the soil grains. The second and third terms represent the advective

209 and conductive heat transport in the subsurface, in which h_l (J/mol) is the specific enthalpy of

210 liquid; $\mathbf{V_l}$ (m/s) is the velocity vector of liquid water determined by Darcy's law; and κ_e (W m^{-1}

211 K^{-1}) is the effective thermal conductivity of the bulk material including soil, air, liquid water, and

212 ice. Q_E is the sum of all thermal energy sources (W/m^3).

213 Similarly, the energy balance equation of the surface system is:

214 $\quad\frac{\partial}{\partial t}\{[\chi\rho_l u_l + (1-\chi)\rho_i u_i]\delta_w\} + \underbrace{\nabla\cdot(h_l\chi\rho_l\delta_w\mathbf{U_w})}_{\text{advective heat}} \underbrace{-\nabla\cdot\{[\chi\kappa_l + (1-\chi)\kappa_i]\delta_w\nabla T\}}_{\text{conductive heat}} = Q_{\text{net}}$ $\qquad$ (6)

215 in which χ is the unfrozen fraction of surface determined by surface temperature; δ_w is ponded

216 depth (m); $\mathbf{U_w}$ (m/s) is the velocity vector of liquid water on the surface determined by the

217 diffusion-wave approximated St. Venant equations (Gottardi and Venutelli, 1993) and Manning

218 equation (Wasantha Lal, 1998); κ_n (W m^{-1} K^{-1}) is the thermal conductivity of n-phase ($n = $ l, i);

219 Q_{net} (W/m^3) is the net thermal energy into and out of ground surface, including that from solar

220 radiation, rain and snow melt, water loss by evaporation and to the subsurface, and conductive and

221 advected heat transport to/from the subsurface. The second and third terms represent the (lateral)

222 advective and conductive heat transport that occur across the land surface.

223 **3 Methods**

224 To evaluate the impact of representation of ice density, cryosuction, and advective heat transport

225 in permafrost modeling under different climate conditions and soil properties, we selected three

226 sites for their variance in climactic condition: Utqiagvik (Barrow Environmental Observatory,

227 71.3225° N, 156.6231° W), the headwaters of the Sagavanirktok (Sag) River (68.251° N, 149.092°

228 W), and the Teller Road Mile Marker 27 site on the Seward Peninsula (64.73° N, 165.95° W) in

229 Alaska. The simulated hydrological outputs for each site are compared in both column and

230 hillslope scenarios. Column scenarios represent expansive flat regions typical of the Arctic coastal

231 plains dominated by vertical infiltration and heat transport, and hillslope scenarios are

232 representative of the headwater, hilly terrain typical of the more inland permafrost.

233 In hillslope scenarios, hillslopes with northern and southern aspects are considered to investigate

234 physics representation comparisons under the same climate and soil condition (i.e., at a given site)

but different solar radiation incidence. Furthermore, hillslopes with both convergent and divergent geometries are included to compare the sensitivity of simulated discharge on process representation. These scenarios can incorporate many types of Arctic systems at the described plot-to-regional scales, but explicitly ignore the effects of microtopography or other local-scale focusing mechanisms such as water tracts or thermo-erosion gullies. The objective is to reach a conclusion on the influence of the three physics representations that can be widely applicable in many Arctic systems.

3.1 Field data description

For each site, data used in each simulation comprises meteorological forcing datasets for the period 2011-2020, averaged wind speed, and soil properties.

Meterological forcing datasets are taken from the Daymet version 4 dataset (Thornton et al., 2020), which provides observation-based, daily averaged weather variables through statistical modeling techniques at 1 km spatial resolution (Thornton et al., 2021). Variables that are used in simulations include daily average air temperature (calculated as the mean of Daymet's daily minimum and maximum values), relative humidity (calculated from air temperature and Daymet's vapor pressure), incoming shortwave radiation (W/m^2) (calculated as a product of Daymet's daylit incoming radiation and daylength), and total precipitation (m/s), which is split into snow and rain based upon the air temperature. Figure 1 illustrates the precipitation of rain, snow, and air temperature at the three sites from 2011 to 2020, where the points represent the corresponding averaged values per year. In terms of the forcing conditions, the annual rainfall of the Sag and Teller sites range between 20 and 40 mm/d over the ten years, more than twice the rainfall typical of the Barrow site. In addition, Sag has a significantly larger amount of snow every year that is over double that at the Teller site and almost five times larger compared to the Barrow site. For the air temperature, Sag and Barrow are similar and colder than Teller by 7-8 degrees. In general, the Barrow site is dry and cold, the Sag site is wet and cold, and the Teller site is wet and warm.
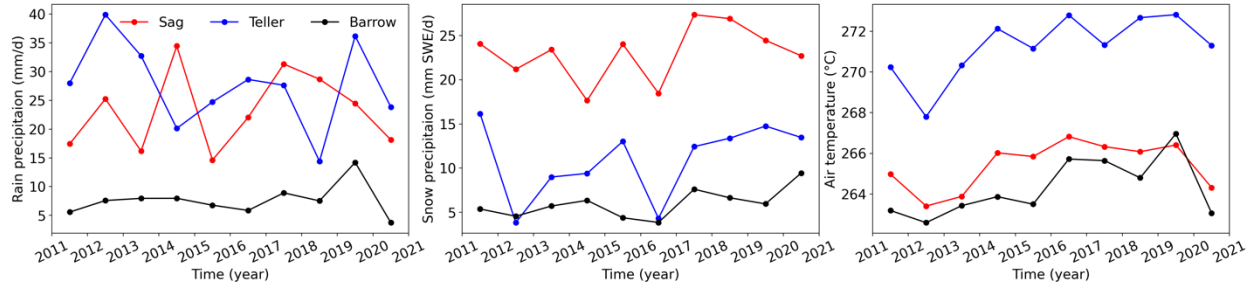
Figure 1 Precipitation and air temperature of site Barrow, Sag, and Teller from year 2011 to 2020

In addition to the time series of forcing data from Daymet, we used an average wind speed for each site. For Barrow and Teller, the average wind speed was estimated from the measurement taken by the Next-Generation Ecosystem Experiments (NGEE) Arctic project. At Barrow, the measurement was taken at area A (71.2815º N, 156.6108 º W) at the height of 1.3 meters above surface (Hinzman et al., 2014). At Teller, the measurement at 3.8 m above the surface of a lower level of the watershed (Busey et al., 2017) was used. For Sag, the average wind speed was estimated based on the measurement at the Toolik Lake field site (near to Sag River) at the height of 3.1 m above surface, which is accessible through the National Ecological Observatory Network (NEON, 2021).

The soil properties of Barrow, Sag, and Teller, including porosity, permeability, Van Genuchten parameters, and thermal conductivity parameters, were chosen from previous modeling studies at these sites (Atchley et al., 2015; Jafarov et al., 2018; O'Connor et al., 2020), see (Table 2). Roughly, the soil profile of each site is composed of two materials: the top organic-rich layer comprising mosses, peats, and other organic rich soils measuring approximately 10-30 cm thick, and the principal mineral soil. There is minor difference in thermal conductivity parameters among the three sites, and soil permeability is also at the same order of magnitude. The soil-water characteristic curve (SWCC) of the principal mineral soil of Barrow, Sag, and Teller, shown in Figure 2, indicates that the soil properties at Barrow and Teller are relatively similar, while Sag differs from the other two with a relatively flat SWCC.
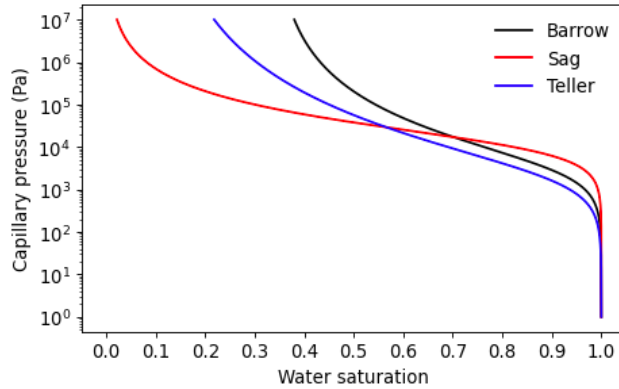
281
282 **Figure 2 Soil-water characteristic curve (SWCC) of soil in Barrow, Sag, and Teller**

283 Usually, at the hillslope scale, the thickness of organic layers of a watershed varies from the toe-
284 slope, through a steeper mid-hill, up to the flat top. Typically, thicker organic layers may exist at
285 the top and bottom compared to the mid-hillslope. The low thermal conductivity of organic layers
286 can impede the heat transport between the air and the underlying mineral soil, resulting in varying
287 thaw depth (or permafrost table depth) along a hillslope, which has been observed at Teller (Jafarov
288 et al., 2018). In this paper, hillslope meshes were constructed following this observation so that
289 the organic layers are thicker at the top and bottom of a hillslope, as described in the next section.

290 **3.2 Mesh design and material properties**

291 The comparison of different physics representations was conducted in both column and hillslope
292 scenarios.
293 The column model was designed as a one-dimensional, 50 m deep domain. The column domain
294 was discretized into 78 cells with gradually increasing cell thickness, starting from 2 cm at the soil
295 surface to 2 m at the bottom of the domain. We assigned different material properties to the cells
296 to represent different soil layers. A column domain is divided into three layers, and the thickness
297 of each layer was designed differently among the three sites according to geological observations
298 (Jan et al., 2020; O'Connor et al., 2020; NGEE-Arctic). Specifically, from top to bottom, the three
299 layers of the Barrow soil column are 2 cm-thick moss, 8 cm-thick peat, and mineral; for Teller, the
300 soil column consists of a 4 cm moss layer, a 22 cm peat layer, and mineral; and the three layers of
301 the Sag soil column are acrotelm, catotelm, with thickness of 10 cm and 14 cm, respectively, and
302 the remainder mineral. The soil properties of each layer at three sites are listed in Table 2.

303 **Table 2 Soil properties of three soil layers of all sites used in this paper**

Site	Barrow			Sag			Teller		
Layers	moss	peat	mineral	acrotelm	catotelm	mineral	moss	peat	mineral
Porosity	0.9	0.876	0.596	0.878	0.796	0.457	0.9	0.55	0.45
Permeability (m^2)	1.7e-11	9.38e-12	6e-13	2.64e-10	9.63e-12	3.98e-13	5e-11	5e-12	2e-13
VG α (Pa^{-1})	2.3e-3	9.5e-4	3.3e-4	7.93e-4	1.75e-4	8.06e-5	2.35e-3	2.93e-4	5.45e-4
VG n	1.38	1.44	1.33	1.405	1.566	1.571	1.38	1.269	1.236
Residual saturation	0.056	0.388	0.334	0.0073	0.0662	0.	0.1	0.	0.1
Thermal conductivity, unfrozen (Wm^{-1}K^{-1})	0.446	0.427	0.788	0.519	0.630	1.309	0.57	0.67	1
Thermal conductivity, dry (Wm^{-1}K^{-1})	0.024	0.025	0.104	0.066	0.086	0.265	0.07	0.07	0.29

304

305 In the hillslope scenario, we designed the mesh based on observations at Teller to represent a
306 generalized, varying-thickness low Arctic hillslope. A hillslope mesh was created first by
307 generating a pseudo-2D surface mesh with 50 cells and then extruding the 2D mesh downward by
308 50 m. The pseudo-2D surface was designed in a trapezoidal shape with a single, variable-width
309 cell in the cross-slope direction to represent convergent/divergent hillslopes, the short and long
310 sides of which are 200 m and 800 m, respectively (see Figure 3). Vertically, from surface
311 downward, the grid size distribution was the same as the column mesh for each site. The domain
312 is also composed of three layers, same as the column, while the numbers of cells representing each
313 soil layer (i.e., soil layer thickness) are different along the hillslope. The thickness distribution of
314 the first two layers of each site is shown in Table 3. The third layer of a hillslope for all sites is the
315 principal mineral soil. Additionally, hillslope meshes with different aspects (i.e., north-facing,
316 south-facing) were also created.
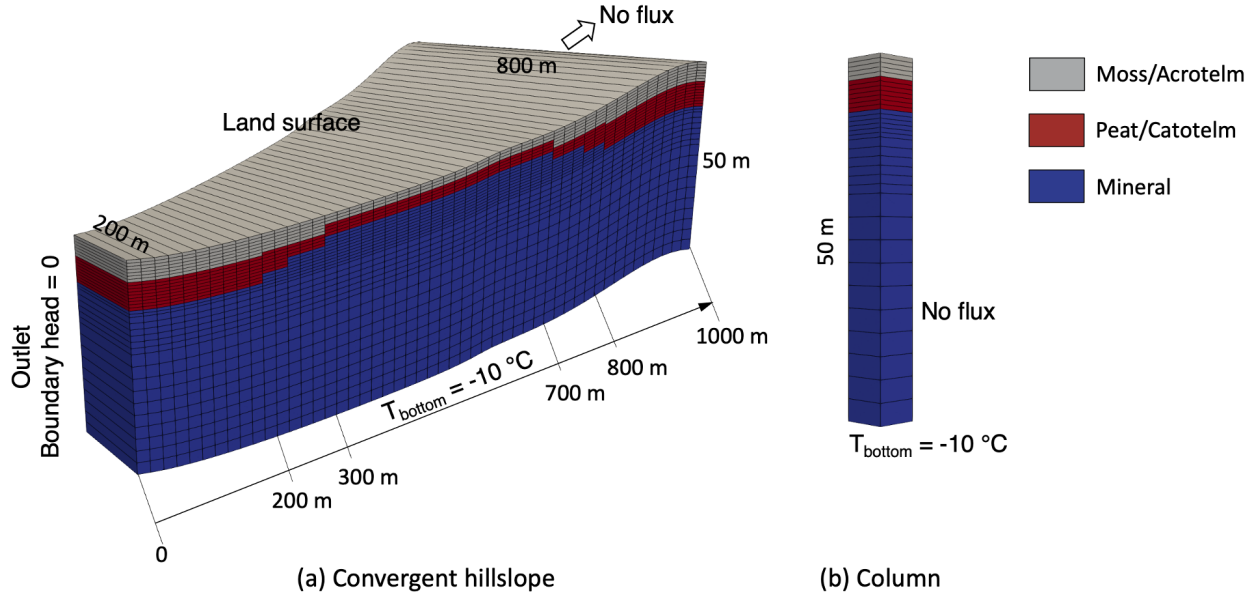
317
318 **Figure 3 Schematic domain mesh and soil layer partition: (a) example of a convergent hillslope domain, (b)**
319 **column domain.**

320 **Table 3 Thickness distribution of the organic layers along hillslope for each site**

Site	Horizontal x range (m)	Barrow layer thickness (cm)	Sag layer thickness (cm)	Teller layer thickness (cm)
Layer 1 Moss/Acrotelm	0 ~ 200	2	14	8
	300 ~ 700	2	6	4
	800 ~ 1000	2	14	8
Layer 2 Peat/Catotelm	0 ~ 200	12	18	22
	300 ~ 700	6	8	22
	800 ~ 1000	12	18	22

321 **3.3 Model setup**

322 To study how the representations of the three physical processes (i.e., ice expansion represented
323 by density, cryosuction, and advective heat transport) affect simulated hydrological outputs at
324 different scales and hillslope topography features, and under various forcing and soil conditions,
325 62 model simulations were conducted, summarized in Table 4. To examine the validity of the
326 assumption of equal density between ice and liquid water, we included cryosuction and advective
327 heat transport in models. To investigate the role of cryosuction in permafrost modeling, we used
328 different density, while neglecting advective heat transport to decrease the computation cost. Note
329 that neglecting advective heat transport in these runs can reduce the effect of cryosuction on
330 simulation predictions, as cryosuction moves water which would itself advect energy. To compare
331 the difference between neglecting and including heat advection, we used different density
332 expressions for ice and liquid, and included cryosuction. Particularly, in order to understand the

333 impact of advective heat transport on permafrost processes when soil is at its wettest, we designed

334 two extreme cases under the warm, wet conditions of the Teller site in which soil evaporation was

335 artificially reduced. These runs were designed to maximize water flux and therefore maximize the

336 potential for advective heat transport to affect predictions.

337

Table 4 Ensemble of models designed in this study

To compare	Site	Scale	Geometry	Aspect	Remark
• $\rho_i \neq \rho_l$, Eq. (1) • $\rho_i = \rho_l$, Eq. (2)	Barrow Sag Teller	column	–	–	• heat advection • cryosuction
		hillslope	convergent	north	
				south	
			divergent	north	
				south	
• Include heat advection • Neglect heat advection	Barrow Sag Teller	column	–	–	• $\rho_i \neq \rho_l$ • cryosuction
		hillslope	convergent	north	
				south	
			divergent	north	
				south	
	Extreme case, Teller	hillslope	convergent	north	• reduced evaporation
• Include cryosuction • Neglect cryosuction	Barrow Sag Teller	column	–	–	• $\rho_i \neq \rho_l$ • no heat advection
		hillslope	convergent	north	
				south	
			divergent	north	
				south	

338

339 Prior to simulating all cases, two steps of initialization are carried out for each site. First, a column

340 model initially above freezing temperature with a given water table depth was frozen by setting

341 the bottom temperature at a constant value of -10 ºC until a steady-state frozen soil column is

342 formed. The initial water table depth is chosen to ensure that the frozen column's water table, after

343 accounting for expansion of ice, is just below the soil surface. The pressure and temperature

344 profiles of the frozen column were used as the initial conditions of the second step initialization.

345 Before proceeding, the observed forcing data (period of 2011-2020) was averaged across the years

346 to form a one-year, "typical" forcing year, which was then repeated 10 times. Using this typical

347 forcing data and the solutions of the first step, we solved the column model in a transient solution,

348 calculating an annual cyclic steady state. The final pressure and temperature profile of the column

349 at the end of the 10-year simulation was then assigned to each column of the hillslope mesh as the

350 initial condition in the formal simulations listed in Table 4. The temperature at the bottom was

351 constant at -10 ºC.

352 **3.4 Evaluation metrics**

353 To fully assess the effect of representation of ice density, advective heat transport, and cryosuction
354 in permafrost hydrology modeling, we used the root mean squared error (RMSE) and normalized
355 Nash–Sutcliffe efficiency (NNSE) as performance metrics. RMSE has the same dimension as the
356 corresponding variables, which can be used to evaluate the average absolute deviation from a
357 benchmark, defined by:

358 $$\text{RMSE} = \sqrt{\frac{\sum_{t=1}^{N}(x_t - y_t)^2}{N}} \tag{7}$$

359 where x_t and y_t are the two modeled datasets to compare from the initial time point ($t = 1$) to the
360 end ($t = N$).

361 NNSE is a normalized dimensionless metric describing the relative relationship between an
362 estimation and a reference, which is oftentimes used for evaluating hydrological models:

363 $$\text{NNSE} = 1/\left(1 + \frac{\sum_{t=1}^{N}(x_t - y_t)^2}{\sum_{t=1}^{N}(x_t - \bar{x})^2}\right) \tag{8}$$

364 where the modeled results x_t (obtained without physics simplification) are considered as the
365 benchmark, and $\bar{x}$ is the mean value of the benchmark. A NNSE approaching 1 indicates perfect
366 correspondence between two groups of values in comparison.

367 In addition, we also used the normalized mean absolute error (MAE) to quantify the percentage
368 change of results obtained with simplified physics relative to full physical representations (see
369 Section 4.4):

370 $$\text{Normalized MAE} = \frac{\sqrt{\sum_{t=1}^{N}|x_t - y_t|/N}}{\text{normalizing reference}} \times 100\% \tag{9}$$

371 Two normalizing references were selected considering different modeled metrics of interest. For
372 instance, in terms of temperature and saturation which fluctuate between two non-zero values, the
373 annually averaged variation range was chosen as the reference:

374 $$\text{Normalizing reference} = \frac{\sum_{\text{year}=1}^{\text{num of years}}(\text{maximum} - \text{minimum})}{\text{number of years}}$$

375 For a modeled metric with zero as the smallest value, such as evaporation, discharge, and thaw
376 depth, the corresponding average value was selected as the reference.

4 Results

378 This section compares simulated outputs over the period of 2011-2020 for the three physical
379 processes under different simulating conditions. We focus on the impact on integrated metrics,
380 such as evaporation, discharge, averaged thaw depth, and depth-dependent metrics, such as

381 temperature, and total water saturation (ice and liquid). For hillslope models, we chose five surface

382 locations according to the slope geometry to collect simulated data, which were then averaged to

383 obtain a single outcome for each metric of interest.

4.1 Ice density

385 To evaluate the representation of ice density on permafrost process simulation, we compared

386 evaporation, discharge, thaw depth, and total water saturation between simulations using equal and

387 different ice density expressions. Figure 4 and Figure 5 show an example of the comparison under

388 conditions of Sag at column and hillslope scales, respectively. Results are compared in both time

389 series and correlation.

390 Generally, at both column and hillslope scales, assuming equal density between ice and liquid has

391 minor impacts on evaporation, discharge, and thaw depth over the 10-year simulation, except at a

392 few deviated points as shown in the correlation figures. According to column-based models, the

393 RMSEs of evaporation, discharge, and thaw depth are 0.101 mm/d, 0.001 m^3/d, and 1.648 cm,

394 respectively, one order of magnitude smaller than the values of the corresponding metrics. At the

395 hillslope scale (see Figure 5) the south-facing divergent hillslope is selected to show modeling

396 comparison on evaporation and thaw depth, in that they are potentially mostly affected when a

397 hillslope has a south orientation and divergent geometry. Likewise, the north-facing convergent

398 hillslope is chosen to compare discharge and water saturation from simulations with different

399 density expressions. Even then, RMSEs of the three metrics are 0.064 mm/d, 111.073 m^3/d, and

400 0.825 cm, respectively, two orders of magnitude smaller than the values of the corresponding

401 metrics at the hillslope scale. Besides, NNSEs of the three metrics output from both column and

402 hillslope simulation are over 0.9, approaching 1 especially at the hillslope scale. Therefore, all

403 indicate good performance of equal ice-liquid density assumption in predicting integrated metrics

404 and thaw depth. By comparison, the estimation of water saturation is relatively more affected by

405 the density assumption during cold seasons within a year, as shown by Figure 4 (d) and Figure 5

406 (d). This is reasonable in that when water mainly exists in the form of ice, equal ice-liquid density

407 assumption will overestimate the water content.
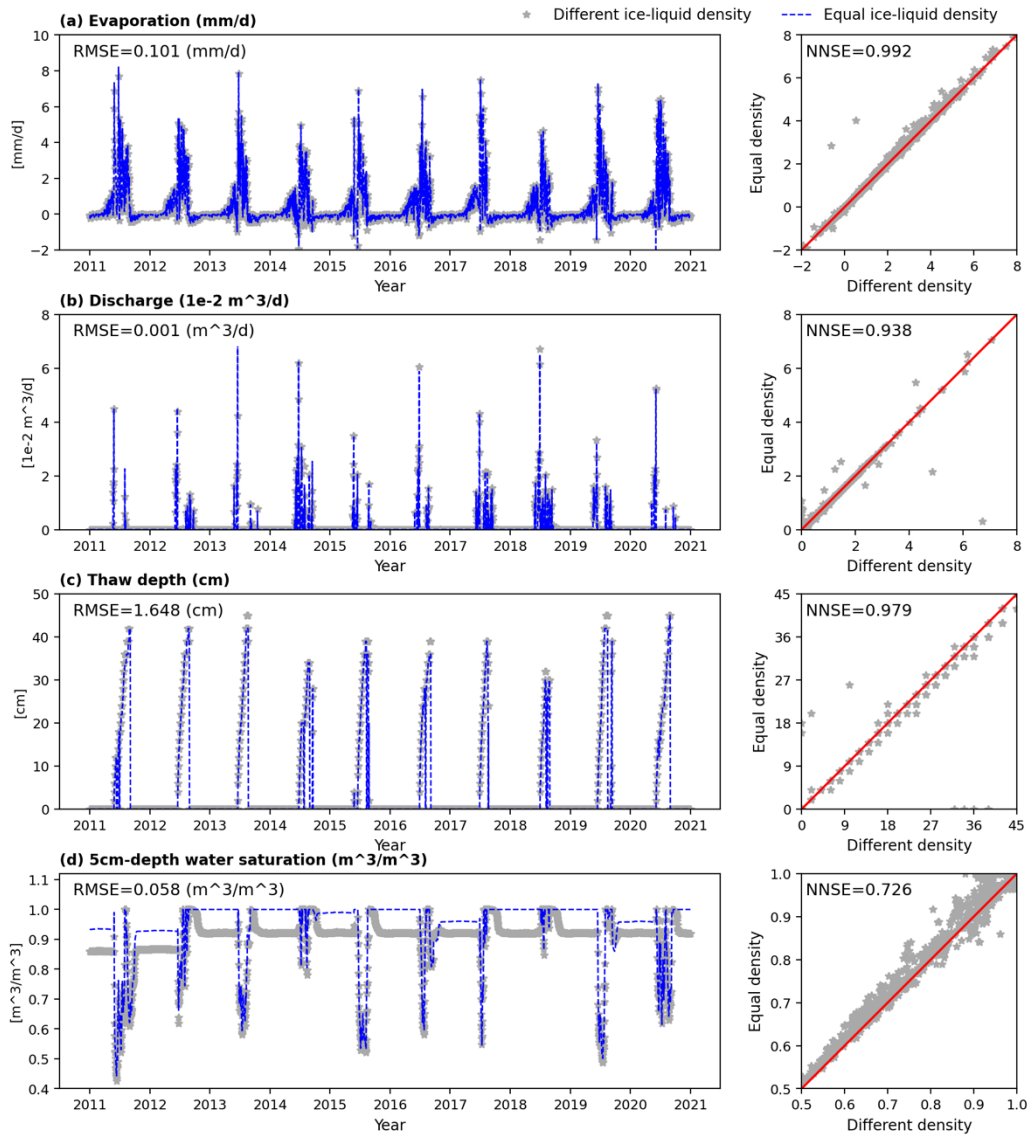
408
409 **Figure 4 Comparison of column simulations between different and equal ice-liquid density under conditions**
410 **of Sag, in (a) evaporation, (b) discharge, (c) thaw depth, and (d) water saturation at 5 cm beneath surface**
411 **from year 2011 to 2020.**
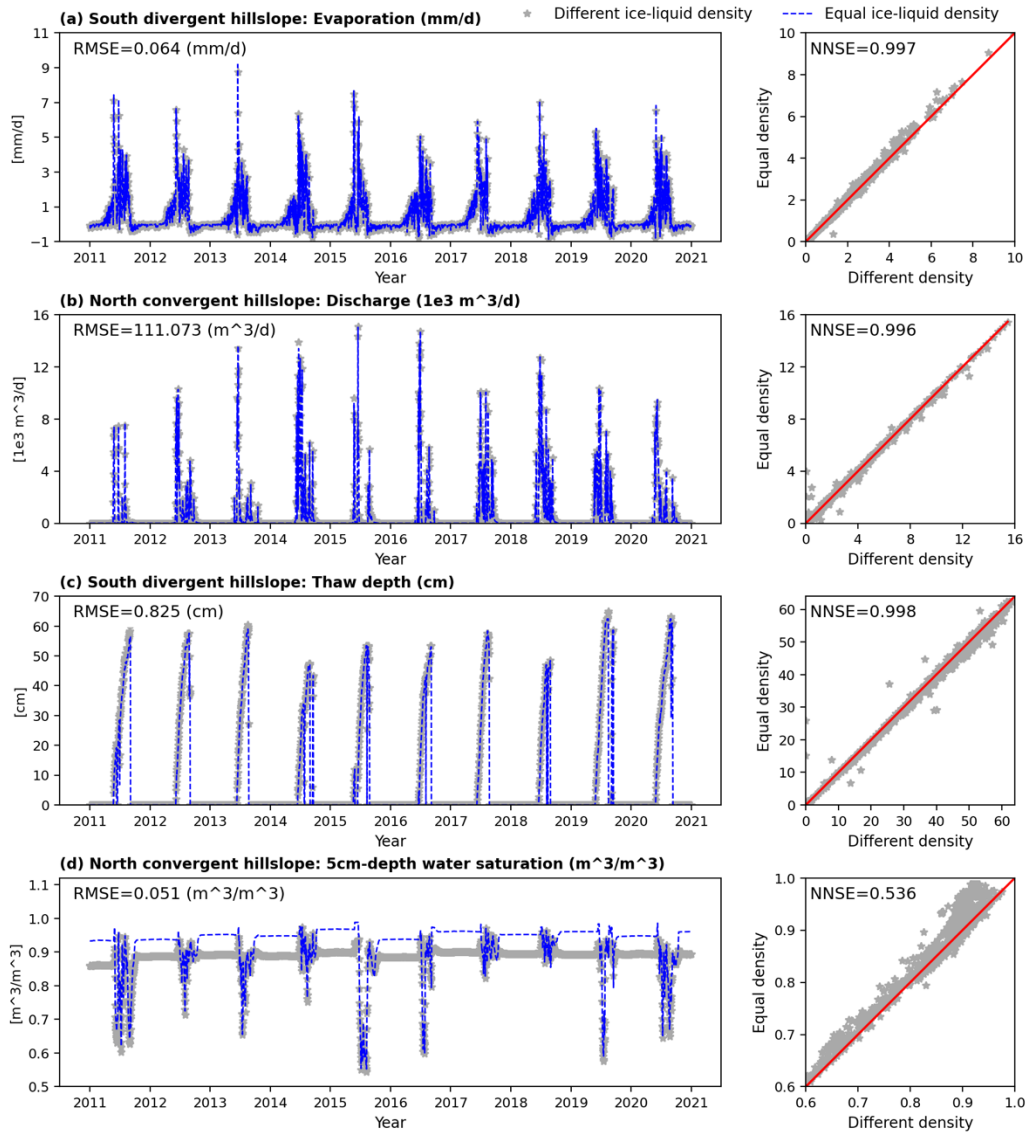
412
413 **Figure 5 Comparison of hillslope simulations between using different and equal ice-liquid density under**
414 **conditions of Sag, in (a) evaporation, (b) discharge, (c) thaw depth, and (d) water saturation at 5 cm beneath**
415 **surface from year 2011 to 2020.**

416 **4.2 Cryosuction**

417 To evaluate the effect of cryosuction on permafrost process predictions, we compared evaporation,

418 discharge, thaw depth, total water saturation, and temperature obtained through simulations

419 including and neglecting cryosuction. Figure 6 through Figure 8 illustrate column-scale

420 comparisons of these metrics under conditions at the three sites (Barrow, Sag, and Teller). Figure

421 6 presents the effect of excluding cryosuction on evaporation and discharge. The RMSE of

422 evaporation from the three sites ranges between 0.25 mm/d and 0.35 mm/d, still one order of

423 magnitude smaller than the common evaporation rate. Evaporation NNSEs of the three sites are

424 around 0.9. For discharge, RMSEs are also one order of magnitude smaller than the average,

425 whereas NNSEs fall between 0.6 and 0.9. Generally, cryosuction plays a more important role in

426 predicting discharge compared to evaporation, especially under warm and wet climate conditions,

427 such as Teller.
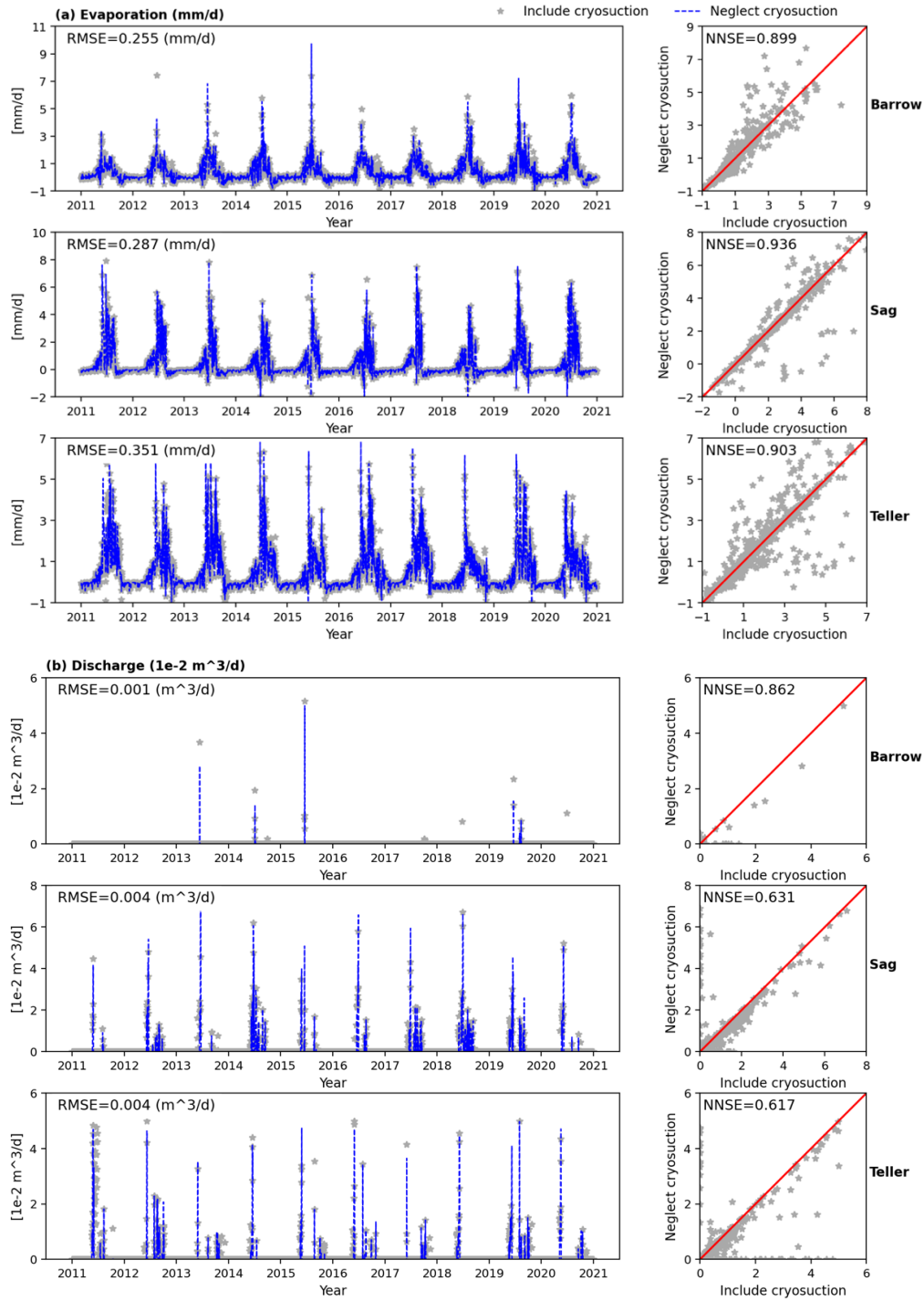
428

429
430 **Figure 6 Comparison of column simulations between including and neglecting cryosuction under conditions**
431 **of Barrow, Sag, and Teller, in (a) evaporation, (b) discharge.**

432 Figure 7 shows the effect of cryosuction on column-scale simulated thaw depth and total water

433 saturation at 5 cm beneath the surface. Overall, neglecting cryosuction tends to underestimate the

434 deepest thaw depth. As already mentioned, cryosuction, in essence, increases soil suction to attract

435 more liquid water moving towards the frozen front during soil freezing. Thus, the real active layer

436 formed due to the existence of cryosuction should be thicker than the cases in which cryosuction

437 is assumed unimportant. RMSEs of thaw depth in Figure 7 range from 3 cm to 8 cm. Though still

438 one order of magnitude smaller than the average annual thaw depth, the estimation error due to

439 neglecting cryosuction is most obvious in summer, especially at areas with cold temperature like

440 Barrow. By comparison, at Teller, where the largest thaw depth is over double that of Barrow and

441 Sag due to its higher temperature, soil cryosuction does not essentially affect thaw depth compared

442 to the other two sites. Similarly, for the total water saturation, at Barrow, the effect of cryosuction

443 is more clearly observed, not only during cold seasons as observed for density representation

444 (section 4.1), but also in summers. The reason why Barrow is more sensitive to the cryosuction

445 process on predicting thaw depth and water content is determined by both soil properties and

446 climate conditions. The soil at Barrow has larger suction and is able to hold more water (see Figure

447 2), providing the possibility for cryosuction to make contributions. Moreover, the principal

448 difference between cryosuction and non-cryosuction representations is presented when the

449 temperature is below the freezing point (see Eq.(3) and Eq.(4)). Compared to Sag and Teller,

450 Barrow has lower annual average temperature (see Figure 1), making the effect of cryosuction

451 more pronounced.

452
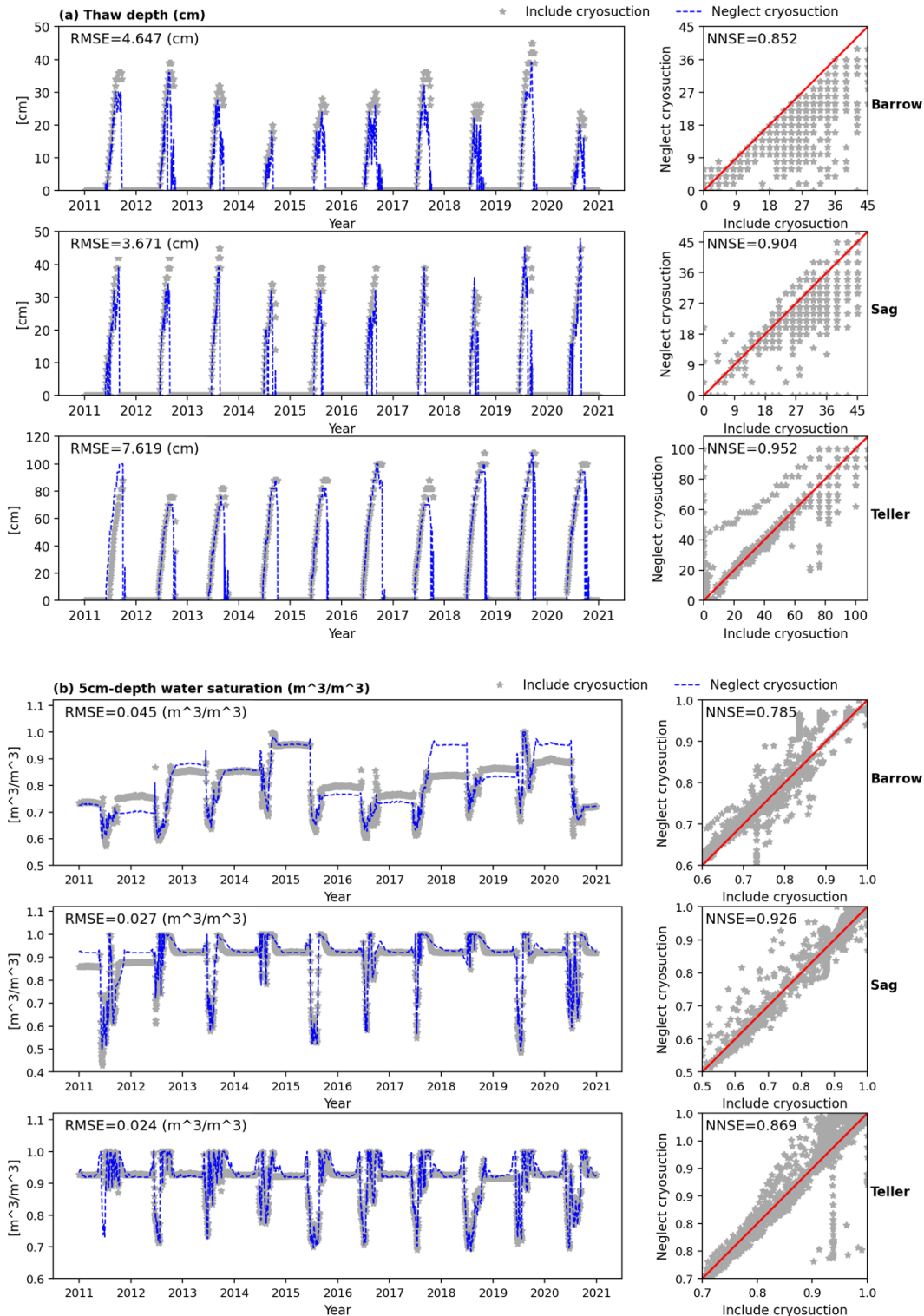
453
Figure 7 Comparison of column simulations between including and neglecting cryosuction under conditions of Barrow, Sag, and Teller, in (a) thaw depth, (b) water saturation at 5 cm beneath surface.

Finally, we also compared soil temperature obtained from models with or without cryosuction in Figure 8. Surface temperature is little affected by cryosuction, except at the Sag site, where the

458 surface temperature is overestimated during winter. At 1 m depth, soil temperature of Barrow is
459 slightly changed in summer due to neglecting cryosuction. At both Sag and Teller, the fluctuation
460 range of temperature at 1 m beneath land surface is underestimated if the cryosuction effect is not
461 considered, especially at Sag, NNSE decreases to approximately 0.6. The reason why Sag and
462 Teller are more sensitive to the effect of cryosuction on temperature is associated with the larger
463 water volume at the two sites. During freezing, soil freezes from ground surface downward and
464 from the bottom of the active layer upward, forming a liquid zone in between where the
465 temperature approximates the freezing point due to phase change (Figure S3.1(a) in the
466 Supplement shows an example of the column model under the Sag River condition at the 300th day
467 of one year). Thus, this liquid zone isolates the upper permafrost from the soil surface temperature
468 variations due to the weakened conductive heat transport along the soil depth. Additionally, the
469 released latent heat in this liquid zone may retard soil freezing, which also tends to reduce thermal
470 conduction. However, cryosuction can speed up freezing and promote the attenuation of the liquid
471 zone (see S3.1(a) and (b) in Supplement. Figure S3.1(b) shows the ice saturation at the same time
472 with Figure S3.1(a), when a soil column still has large non-frozen area), which thus decrease the
473 impact of the liquid zone. Hence, the influence of cryosuction is more significant with more soil
474 water.
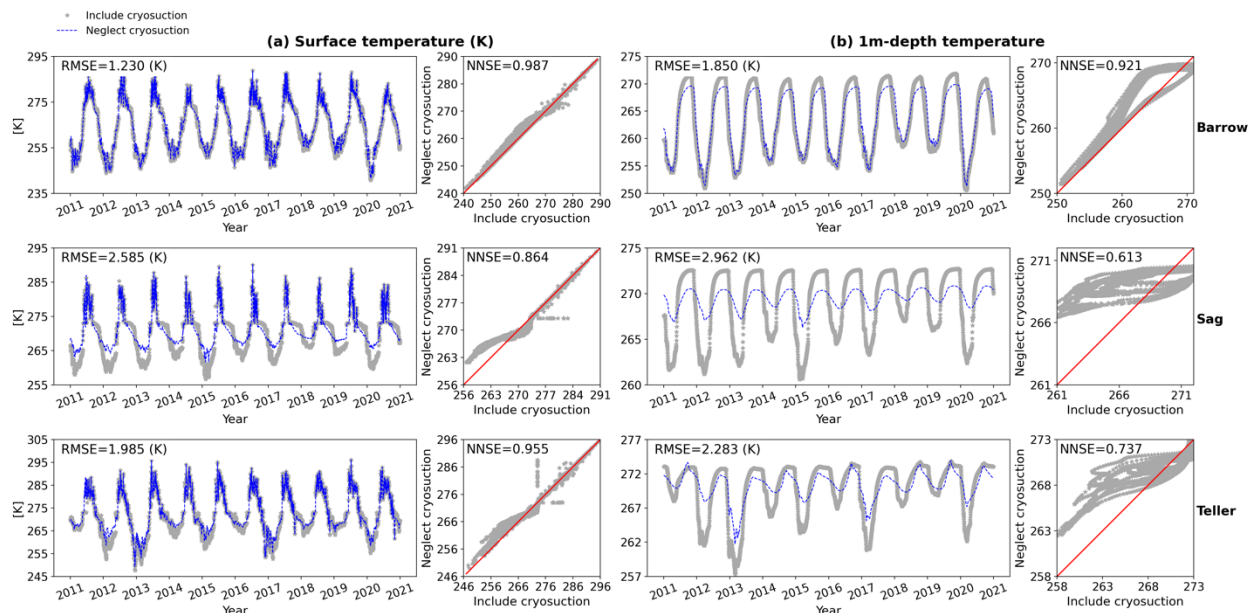
476 **Figure 8 Comparison of column simulations between including and neglecting cryosuction under conditions**
477 **of Barrow, Sag, and Teller, in (a) surface temperature, (b) temperature at 1 m beneath surface.**

478 Therefore, from Figure 6 to Figure 8, neglecting the cryosuction effect in column-scale simulations

479   has less impact on integrated hydrological metrics, but will cause significant difference when

480   estimating thaw depth and location-specific metrics. The difference among these metrics varies

481   under different climate conditions. Integrated metrics, such as evaporation and discharge, are

482   affected more under warm and wet conditions (Teller); thaw depth and water saturation are

483   affected more under cold and low-rainfall conditions (Barrow); and soil temperature tends to be

484   affected more under cold and high precipitation (rain and snow) conditions (Sag).

485   Neglecting soil cryosuction has a similar impact on hydrological outputs in hillslope scale models.

486   Figure 9 shows the comparison of the metrics of interest discussed above under the Sag climate.

487   Evaporation, thaw depth, and temperature are presented based on south-facing divergent hillslope

488   models, while discharge and water saturation are from hillslope models with north-facing

489   convergent geometry. In general, neglecting soil cryosuction has a smaller effect on integrated

490   metrics (evaporation and discharge) compared with other pointwise metrics. Though thaw depth

491   presents a high NNSE of approximately 0.94, and low RMSE of about 4.5 cm compared to the

492   average, indicating a good match between models considered and excluded cryosuction, the

493   estimation error during summer may reach as high as 10 cm, particularly from 2011 to 2017, as

494   shown in Figure 9 (c). Obvious errors in water saturation and temperature, similar with column-

495   scale models, occur almost annually with respect to extrema during winter and summer. Overall,

496   compared to column-scale models, differences in evaporation, discharge, thaw depth, and surface

497   temperature due to neglecting cryosuction are relatively reduced at the hillslope scale if comparing

498   NNSEs (Table 5). Localized subsurface metrics, such as water saturation and 1m-depth soil

499   temperature, show increased errors from column to hillslope scale models, which is primarily

500   caused by lateral flux exchange captured by hillslope modeling.

501
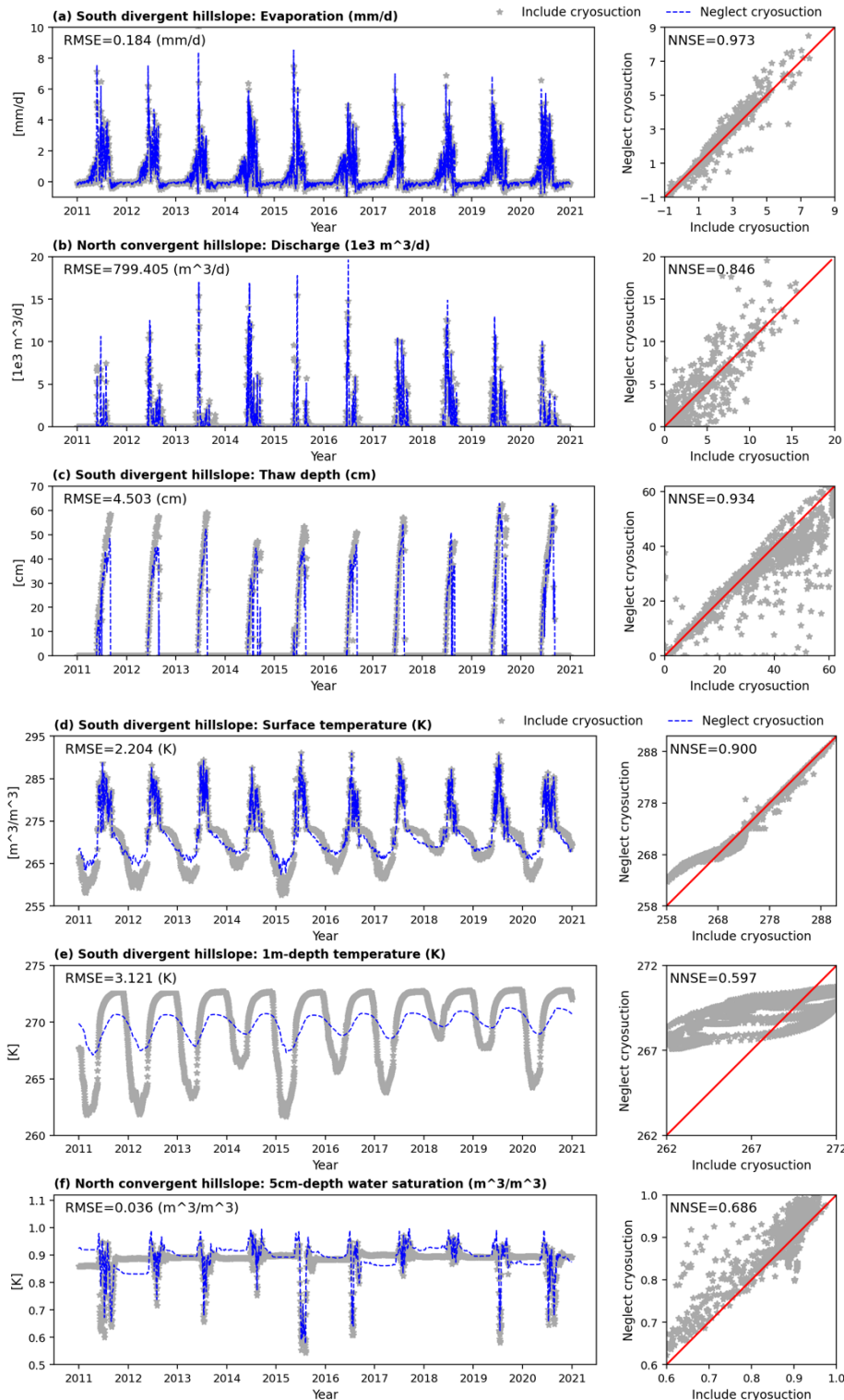
502
503 **Figure 9 Comparison of hillslope simulations between including and neglecting cryosuction under conditions**
504 **of Sag, in (a) evaporation, (b) discharge, (c) thaw depth, (d) water saturation at 5 cm beneath surface, (e)**
505 **surface temperature, (f) temperature at 1 m beneath surface.**

Table 5 NNSE of outputs from column and hillslope models under conditions of Sag shown in Figure 6 through Figure 9

Scale	Evaporation (mm/d)	Discharge (m³/d)	Thaw depth (cm)	5cm-depth water saturation (-)	Surface temperature (K)	1m-depth temperature (K)
Column	0.936	0.631	0.904	0.926	0.864	0.613
Hillslope	0.973	0.846	0.934	0.686	0.900	0.597

4.3 Advective heat transport

This section evaluates the performance of advective heat transport in modeling permafrost process. As above, we investigated the influence of neglecting heat advection on evaporation, discharge, thaw depth, total water saturation, and temperature. Overall, after comparing all hydrological outputs from models with different heat transport representations, heat advection is proved insignificant in an Arctic system where the influence of localized groundwater flow can be neglected. Comparisons based on column-scale and hillslope-scale models are not shown here (see Supplement); instead, the extreme case under conditions of Teller is presented (Figure 10). Teller is abundant in rainfall over the period of 2011-2020 (Figure 1). In the extreme case, evaporation was reduced artificially to almost a quarter of the original value (see Figure 6 (a) at Teller and Figure 10 (a)) for the purpose of increasing water flow rates. For instance, discharge has quadrupled after adjusting evaporation by comparing Figure 10 (b) and Figure 6 (b) at Teller. This specific scenario is chosen to maximize the potential effect of advective heat transport in a hillslope-scale Arctic system. Figure 10 illustrates comparisons on all outputs mentioned above from hillslope models without heat advection and with full thermal representation. Apparently, all RMSEs are extremely small, at least two orders of magnitude lower than the corresponding metric average. Almost all NNSEs are approximately one, even for thaw depth, localized water saturation, and temperature. Under the assumption of large-scale Arctic systems ignoring the influence by localized groundwater flow features (e.g., ponds, gullies, etc.), the liquid water flux determines the advective heat transport in the subsurface. However, the flow velocity on average is quite low within the shallow active layer with limited thickness (see Figure S4.1 in Supplement). As a consequence, the advective heat transport only makes contributions within the top shallow layers, and the relatively larger advective heat flux is lower than the conductive heat flux over one order of magnitude (see Figure S4.2 in Supplement). Therefore, for such large-scale Arctic systems where localized groundwater flow makes less contributions, it is reasonable to neglect advective heat transport.
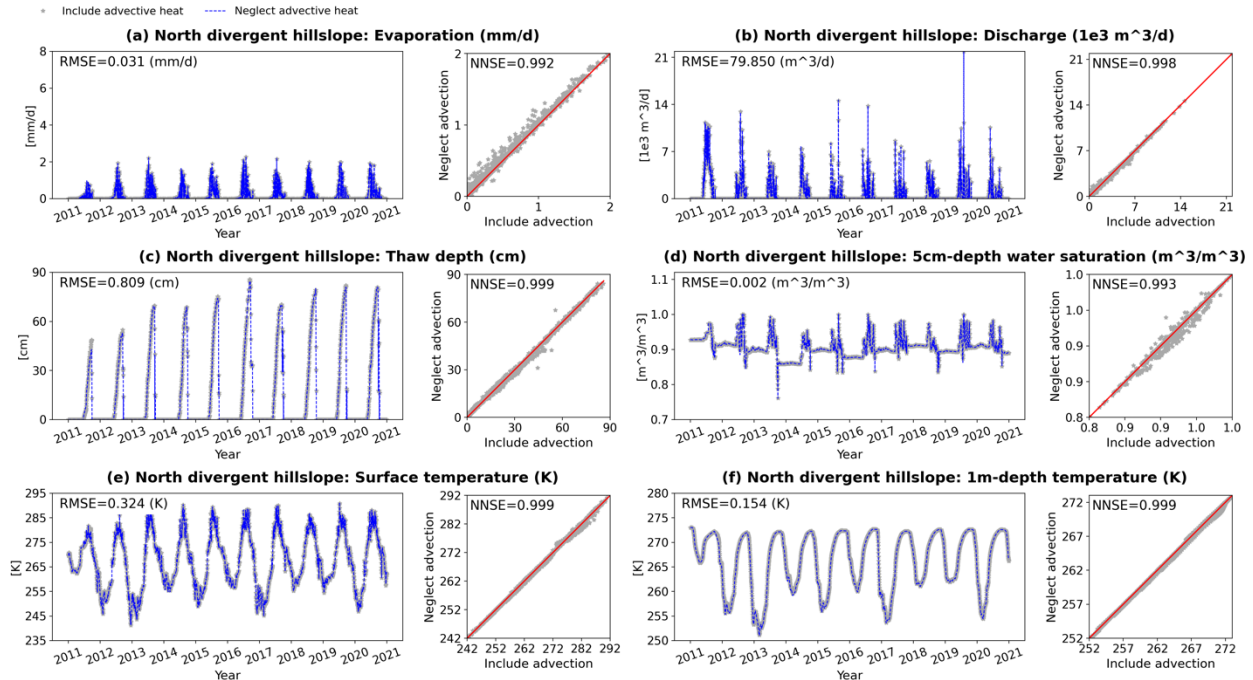
534
535 **Figure 10 Comparison of hillslope simulations between including and neglecting advective heat transport**
536 **under extreme conditions of Teller, in (a) evaporation, (b) discharge, (c) thaw depth, (d) water saturation at 5**
537 **cm beneath surface, (e) surface temperature, (f) temperature at 1 m beneath surface**

538 **4.4 Comprehensive comparison**

539 In the above three sections, we discussed time-series simulation comparisons. This section will

540 analyze the effect of equal ice-liquid density, neglecting cryosuction, and neglecting heat

541 advection on permafrost modeling outputs from holistic, average perspectives.

542 First, we extracted NNSEs of all the metrics of interest obtained from all comparing models for

543 qualitative analysis. Table 6 shows an example based on column-scale models under conditions of

544 three different sites. Red numbers highlight the obviously reduced NNSEs of one or two processes

545 among the three for each metric. Overall, neglecting advective heat transport has the least influence

546 on model outputs. Equal ice-liquid density primarily affects saturation and has less effect on other

547 metrics. Excluding soil cryosuction makes the greatest impact on almost all metrics, especially in

548 a relatively wet environment. Among these metrics, evaporation and surface temperature are less

549 affected by the three physical process representations, while location-based water saturation is

550 most affected.

551 **Table 6 A summary of NNSEs of metrics of interest obtained through column model comparison**

Metrics	Barrow			Sag			Teller		
	Heat	*Ice*	*Cryosuction*	*Heat*	*Ice*	*Cryosuction*	*Heat*	*Ice*	*Cryosuction*

	advection	density		advection	density		advection	density	
Evaporation	0.997	0.994	0.899	0.993	0.992	0.937	0.999	0.996	0.903
Discharge	0.924	0.628	0.862	0.996	0.938	0.631	0.985	0.987	0.618
Thaw depth	0.997	0.996	0.852	0.991	0.979	0.904	0.997	0.989	0.952
5cm-depth s_w	0.996	0.934	0.785	0.992	0.726	0.926	0.998	0.562	0.869
40cm-depth s_w	0.993	0.022	0.213	0.995	0.062	0.311	0.999	0.281	0.850
Surface T	1.000	1.000	0.987	0.999	0.999	0.864	1.000	1.000	0.955
1m-depth T	1.000	1.000	0.921	1.000	1.000	0.613	1.000	0.999	0.737

552 * s_w and T in Table 6 are water saturation and temperature, respectively.

553 Furthermore, to quantitively compare across the physical processes, we calculated the mean

554 absolute error (MAE) for each metric of interest over the simulation period of 2011-2020. For

555 evaporation, discharge, and thaw depth, the MAEs are normalized by the corresponding metric

556 average (numbers in Figure 11 (a)); for water saturation and temperature, the MAEs are normalized

557 by their average annual fluctuation range (numbers in Figure 11 (b)). All normalized MAEs are

558 presented in percentage, displayed in Figure 11 according to column- and hillslope-scale (e.g.,

559 south-facing convergent hillslope) models under three different climate conditions. Hillslope-scale

560 model output under conditions of Barrow is not shown in that flat land occupies a majority of the

561 area. A larger normalized MAE percentage indicates greater impact on the metric resulted from a

562 physical process.

563 From the perspective of 10-year average, in general, each physical process of Arctic systems

564 discussed in this paper presents a similar impact on metrics between column and hillslope scales.

565 Under climate and soil conditions of three different sites, neglecting cryosuction in permafrost

566 modeling leads to the greatest influence on hydrological prediction amongst the three physical

567 assumptions. As seen in Figure 11 (a), it will result in 10% ~ 20% deviation in evaporation, 50%

568 ~ 60% in discharge, and 10% ~ 30% in thaw depth. Evaporation is the least affected among the

569 three metrics. Discharge is more affected in regions with abundant rainfall (Teller), while in

570 regions with less precipitation, evaporation and thaw depth are relatively affected (Barrow). By

571 comparison, assuming equal ice-liquid density and neglecting advective heat transport may only

572 cause 10% and 5% or even much lower error, respectively, in reference to the annual average of a

573 metric. Specially in Barrow, models utilizing the same ice and liquid densities and ignoring

574 advective heat transport seem to make an obvious impact on discharge, whereas this also results

575 from its extremely low discharge (Figure 6 (b)).

576 Figure 11 (b) illustrates the normalized MAEs of water saturation at 5 cm beneath surface, as well

577 as temperature at surface and 1 m depth. The assumption of equal ice-liquid density primarily

578 affects the estimation of the water saturation profiles, which can lead to about 5% ~ 15% error

579 relative to the annual change range, and the error percentage tends to slightly decrease when

580 applying hillslope-scale models due to the inclusion of lateral flow. Apart from this, neglecting

581 soil cryosuction still makes the largest impact. Surface temperature is the least affected metric

582 among all these model outputs even if cryosuction is not included in modeling. However, at 1 m

583 depth, error can increase to 10% ~ 30% by simulation without cryosuction representation.
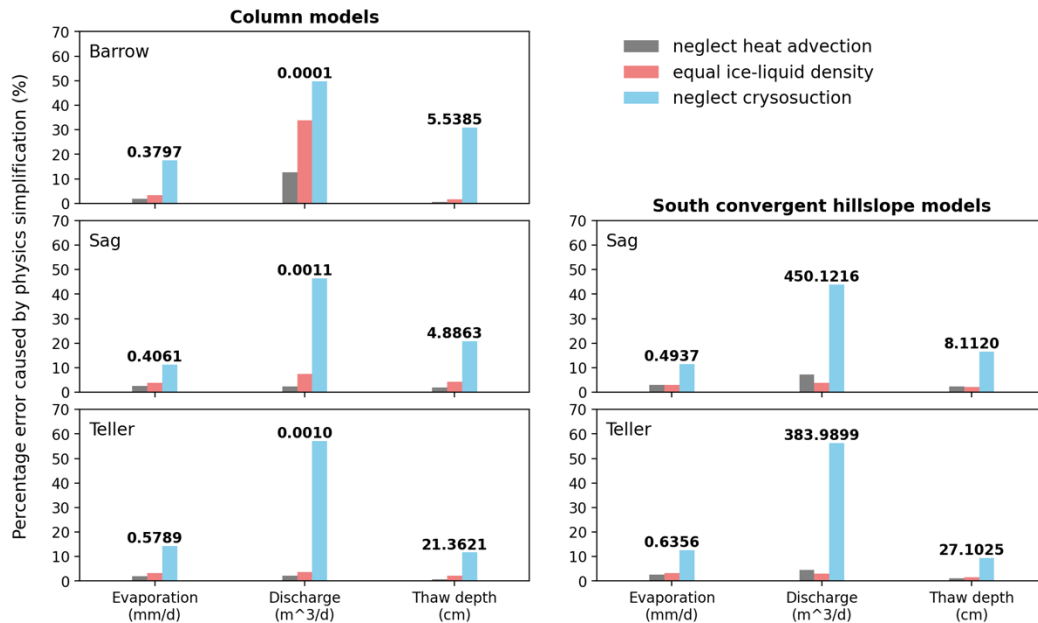
584
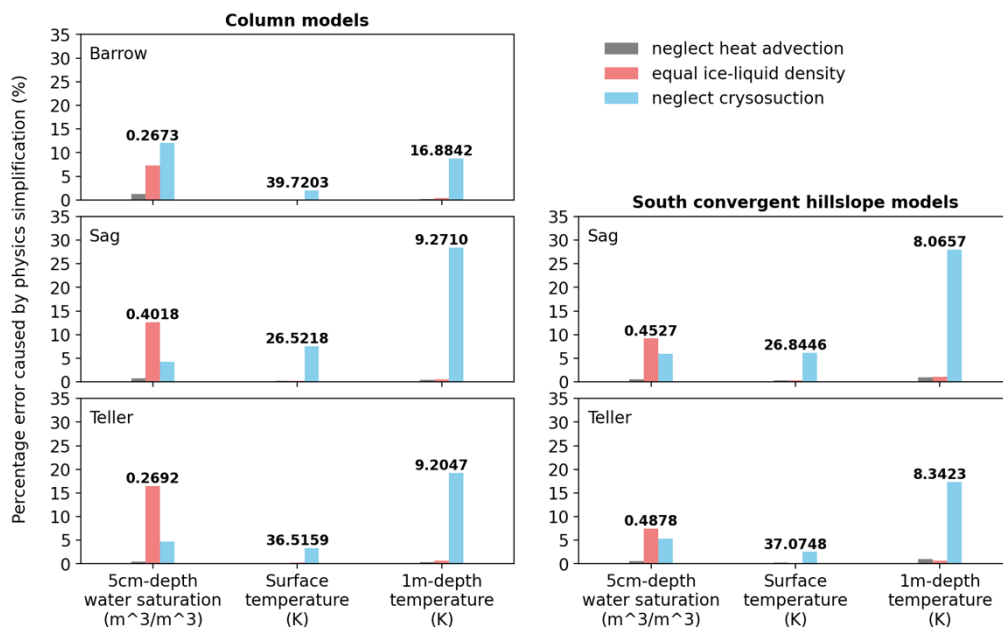
585
586 **Figure 11 Percentage errors for each metric caused by physics simplifications at column and hillslope scales.**

587 **The percentage error refers to the averaged error of a metric over the period of 2011-2020 normalized by a**
588 **certain reference value obtained from full-physics model. Metrics include (a) evaporation, discharge, and**
589 **thaw depth; (b) water saturation, and temperatures. Numbers in figures are the corresponding reference**
590 **values for each metric: (a) 10-year average obtained from full-physics model; (b) 10-year averaged annual**
591 **fluctuation range obtained from full-physics model.**

592 **5 Conclusion**

593 The premise of this study is, by starting from general mass and energy transport equations and

594 simplifying the process representations, we can use a process-rich model to understand the relative

595 importance of given process simplifications in describing permafrost hydrology. This process

596 sensitivity analysis, performed at the scale of field sites as opposed to previous studies at smaller

597 scales such as lab experiments, provides improved understanding in the processes governing

598 permafrost hydrology at this scale. As the simplifications considered here largely span the

599 equations considered in a class of process-rich models, this process sensitivity analysis is relevant

600 to model developers across a range of codes.

601 Simplification of Arctic process representation is an essential consideration when developing

602 process-rich models for thermal permafrost hydrology. The following three subsurface process

603 simplifications are commonly applied for many Arctic tundra models: (i) ice is prescribed the same

604 density as liquid water; (ii) the effect of soil cryosuction is neglected; (iii) advective heat transport

605 is neglected. Here we investigated the influence of these simplified representations on modeling

606 field-scale permafrost hydrology in a set of simplified geometries commonly used in the

607 permafrost hydrology literature with the Advanced Terrestrial Simulator (ATS v1.2). We note that

608 these conclusions are specific to conditions similar to these geometries, and should not be applied

609 in cases where focusing flow mechanisms may dominate.

610 To do this, we conducted an ensemble of simulations to evaluate the impact of the above three

611 process simplifications on field-scale predictions. The ensemble of simulations consisted of 62

612 numerical experiments considering various conditions, including different climate conditions and

613 soil properties at three sites of Alaska, and different model scale conceptualizations. For evaluation,

614 we compared integrated metrics (evaporation, discharge), averaged thaw depth, and pointwise

615 metrics (temperature, total water saturation), which are of general interest, among different models

616 to access the deviation of applying a simplified modeling assumption. The main conclusions, under

617 the assumed conditions in this study, are summarized as follows:

618   1) Excluding soil cryosuction can cause significant bias on estimation of most hydrological

619   metrics at field-scale permafrost simulations. In particular, under the assumed conditions,

620   the average deviation in evaporation, discharge, and thaw depth may reach 10% ~ 20%,

621   50% ~ 60%, and 10% ~ 30%, respectively, relative to the corresponding annual average

622   values. The prediction error for discharge may grow if rainfall rates increase. In the case

623   of pointwise metrics, the error in temperature increases from a small amount at the surface

624   up to 10% ~ 30% at 1 m beneath surface. The prediction of subsurface temperature and

625   water saturation is especially affected when considering hillslope scale models. Therefore,

626   soil cryosuction should be included when modeling permafrost change.

627   2) Assuming equal ice-liquid density will not result in especially large deviations when

628   predicting most of the hydrological metrics, particularly at hillslope scales given all cases

629   in this study. It primarily affects the prediction of the soil water saturation profile and can

630   cause 5% ~ 15% error relative to the annual saturation fluctuation range. This difference

631   may have consequences for the carbon cycle with regards to the production of methane

632   versus carbon dioxide. Assigning liquid water density for ice may reduce computational

633   time to a small extent in ATS, dependent on simulating conditions and spatial and temporal

634   scales.

635   3) For a large-scale Arctic tundra system with limited localized groundwater flow features

636   (e.g., taliks, thermo-erosion gullies, etc.), the prediction error in most metrics of interest

637   after neglecting advective heat transport is less than 5%, or even much lower. In the case

638   of ATS, the simulation time cost for hillslope-scale models can decrease by 40% to 80%

639   under conditions in this study. Ignoring heat advection in the absence of local, flow-

640   focusing mechanisms, such as thermo-erosion gullies, seems a reasonable decision.

641 Through the comparison of permafrost hydrological outputs obtained from ensemble model setups

642 targeted at the field scale, we confirm the importance and necessity of including soil cryosuction

643 in predicting permafrost changes, and validate the application of equal ice-liquid density and

644 neglecting advective heat transport for an Arctic system where localized groundwater flow is not

645 a dominant feature. The latter two may also ease computational cost dependent upon simulation

646 conditions. We expect that this study can contribute to the development of permafrost hydrology

647 models, as well as better selection of physical process representations for modelers, and better

648 understanding of permafrost physics for the community.

Appendix

The following results may provide some information about computation cost for ATS users. In addition to the influence of process representations on permafrost hydrology metrics of general interest, we also investigated how much the simplified processes can affect the runtime of a model at the hillslope scale.

First, using the 10-year simulation with real ice density as references, the percentage change of time consumed after applying equal ice-liquid density was calculated and displayed in Figure A1. Overall, under the equal density assumption, it may take less time (positive values in figure), but no more than 25% and on average lower than 10%. However, the computation time may also increase (negative values in figure) under wet conditions, such as at Sag and Teller. Thus, given a long-period modeling of large-scale permafrost system, there is no consistent conclusion on whether equal ice-liquid density can ease computational cost. It depends on both the weather conditions and soil properties.

Figure A1. The relative runtime change in percentage due to the assumption of equal ice-liquid density compared to that with the real ice density representation for all hillslope scale models.

Second, section 4.2 has demonstrated that neglecting cryosuction will make a great impact on hydrological estimations. As a significant physical process of permafrost, cryosuction should be implemented in numerical models even if additional computation effort is potentially required. However, based on the hillslope models we conducted, including cryosuction does not necessarily raise computational cost, which also depends on specific soil properties and conditions. The cases that consume more time after considering cryosuction effect just increase the time by 10% ~ 30%, and less than 20% on average (see Figure A2).

672
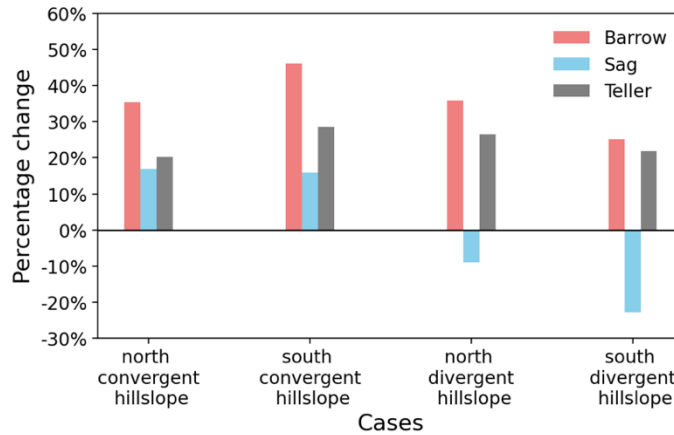
Figure A2. The relative runtime change in percentage after neglecting cryosuction compared to the cases with cryosuction for all hillslope scale models.

Third, in terms of heat advection, ATS uses the Algebraic Multigrid method as preconditioner for solving, which has a relatively deficient performance in dealing with hyperbolic equations. Thus, incorporating advective heat transport will aggravate computational cost, particularly in case of both large spatial and temporal scales. Figure A3 shows the relative percentage reduction in computational time for 10-year simulations after excluding heat advection in both surface and subsurface thermal flux. It drops by 70% ~ 80% under wet conditions (e.g., Sag and Teller) and 40% ~ 60% under dry conditions (e.g., Barrow). Hence, neglecting advective heat transport considerably improves the performance of large spatial-temporal permafrost hydrology simulations.
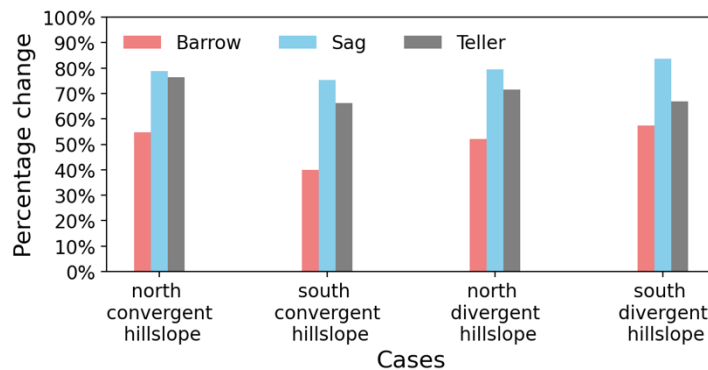
684
685 **Figure A3. The relative runtime change in percentage due to the neglect of advective heat transport for all**
686 **hillslope scale models.**

Code availability

Advanced Terrestrial Simulator (ATS) is an open-source code for solving ecosystem-based, integrated, distributed hydrology, and available at https://github.com/amanzi/ats. Simulations were

690 conducted using version 1.2 (Coon et al., 2021).

Data availability

Data sources of wind speed are cited in the text. The raw forcing data acquired from Daymet, the processed forcing data used for simulation, and simulation output data are available through https://github.com/gaobhub/data_for_paper_model_comparison.

Author contributions

Bo Gao did some revision of the code to add options for process representations, designed numerical experiments and setup models, did data analysis and interpretation, drafted and revised the article. Ethan T. Coon implemented the code in which the study was done, conceptualized the study, helped debug the runs, and helped draft and revise the article.

Competing interests

The authors declare that they have no conflict of interest.

Acknowledgement

Both authors are supported by the U.S. Department of Energy, Office of Science, Biological and Environmental Research program under the InteRFACE project. This research used resources of the Compute and Data Environment for Science (CADES) at the Oak Ridge National Laboratory, which is supported by the Office of Science of the U.S. Department of Energy under Contract No. DE-AC05-00OR22725.

References

Abolt, C. J., Young, M. H., Atchley, A. L., Harp, D. R., and Coon, E. T.: Feedbacks Between Surface Deformation and Permafrost Degradation in Ice Wedge Polygons, Arctic Coastal Plain, Alaska, J. Geophys. Res. Earth Surf., 125, e2019JF005349, https://doi.org/10.1029/2019JF005349, 2020.

Atchley, A. L., Painter, S. L., Harp, D. R., Coon, E. T., Wilson, C. J., Liljedahl, A. K., and Romanovsky, V. E.: Using field observations to inform thermal hydrology models of permafrost dynamics with ATS (v0.83), Geosci. Model Dev., 8, 2701–2722, https://doi.org/10.5194/gmd-8-

716   2701-2015, 2015.

717   Berteaux, D., Gauthier, G., Domine, F., Ims, R. A., Lamoureux, S. F., Lévesque, E., and Yoccoz,
718   N.: Effects of changing permafrost and snow conditions on tundra wildlife: critical places and
719   times, Arct. Sci., 3, 65–90, https://doi.org/10.1139/as-2016-0023, 2017.

720   Bui, M. T., Lu, J., and Nie, L.: A Review of Hydrological Models Applied in the Permafrost-
721   Dominated Arctic Region, Geosciences, 10, 401, https://doi.org/10.3390/geosciences10100401,
722   2020.

723   Busey, B., Bolton, B., Wilson, C., and Cohen, L.: Surface Meteorology at Teller Site Stations,
724   Seward Peninsula, Alaska, Ongoing from 2016, 2017.

725   Chen, L., Fortier, D., McKenzie, J. M., and Sliger, M.: Impact of heat advection on the thermal
726   regime of roads built on permafrost, Hydrol. Process., 34, 1647–1664,
727   https://doi.org/10.1002/hyp.13688, 2020.

728   Cheng, G. and Wu, T.: Responses of permafrost to climate change and their environmental
729   significance, Qinghai-Tibet Plateau, J. Geophys. Res. Earth Surf., 112,
730   https://doi.org/10.1029/2006JF000631, 2007.

731   Coon, E. T., David Moulton, J., and Painter, S. L.: Managing complexity in simulations of land
732   surface and near-surface processes, Environ. Model. Softw., 78, 134–149,
733   https://doi.org/10.1016/j.envsoft.2015.12.017, 2016.

734   Coon, E. T., Moulton, J. D., Kikinzon, E., Berndt, M., Manzini, G., Garimella, R., Lipnikov, K.,
735   and Painter, S. L.: Coupling surface flow and subsurface flow in complex soil structures using
736   mimetic finite differences, Adv. Water Resour., 144, 103701,
737   https://doi.org/10.1016/j.advwatres.2020.103701, 2020.

738   Dagenais, S., Molson, J., Lemieux, J.-M., Fortier, R., and Therrien, R.: Coupled cryo-
739   hydrogeological modelling of permafrost dynamics near Umiujaq (Nunavik, Canada), Hydrogeol.
740   J., 28, 887–904, https://doi.org/10.1007/s10040-020-02111-3, 2020.

741   Dall'Amico, M., Endrizzi, S., Gruber, S., and Rigon, R.: A robust and energy-conserving model
742   of freezing variably-saturated soil, The Cryosphere, 5, 469–484, https://doi.org/10.5194/tc-5-469-
743   2011, 2011.

744   Dearborn, K. D., Wallace, C. A., Patankar, R., and Baltzer, J. L.: Permafrost thaw in boreal
745   peatlands is rapidly altering forest community composition, J. Ecol., 109, 1452–1467,
746   https://doi.org/10.1111/1365-2745.13569, 2021.

747   Devoie, É. G. and Craig, J. R.: A Semianalytical Interface Model of Soil Freeze/Thaw and
748   Permafrost Evolution, Water Resour. Res., 56, e2020WR027638,
749   https://doi.org/10.1029/2020WR027638, 2020.

750   Endrizzi, S., Gruber, S., Dall'Amico, M., and Rigon, R.: GEOtop 2.0: simulating the combined
751   energy and water balance at and below the land surface accounting for soil freezing, snow cover

752 and terrain effects, Geosci. Model Dev., 7, 2831–2857, https://doi.org/10.5194/gmd-7-2831-2014,
753 2014.

754 Fortier, D., Allard, M., and Shur, Y.: Observation of rapid drainage system development by
755 thermal erosion of ice wedges on Bylot Island, Canadian Arctic Archipelago, Permafr. Periglac.
756 Process., 18, 229–243, https://doi.org/10.1002/ppp.595, 2007.

757 Godin, E., Fortier, D., and Coulombe, S.: Effects of thermo-erosion gullying on hydrologic flow
758 networks, discharge and soil loss, Environ. Res. Lett., 9, 105010, https://doi.org/10.1088/1748-
759 9326/9/10/105010, 2014.

760 Gottardi, G. and Venutelli, M.: A control-volume finite-element model for two-dimensional
761 overland flow, Adv. Water Resour., 16, 277–284, https://doi.org/10.1016/0309-1708(93)90019-C,
762 1993.

763 Grenier, C., Anbergen, H., Bense, V., Chanzy, Q., Coon, E., Collier, N., Costard, F., Ferry, M.,
764 Frampton, A., Frederick, J., Gonçalvès, J., Holmén, J., Jost, A., Kokh, S., Kurylyk, B., McKenzie,
765 J., Molson, J., Mouche, E., Orgogozo, L., Pannetier, R., Rivière, A., Roux, N., Rühaak, W.,
766 Scheidegger, J., Selroos, J.-O., Therrien, R., Vidstrand, P., and Voss, C.: Groundwater flow and
767 heat transport for systems undergoing freeze-thaw: Intercomparison of numerical simulators for
768 2D test cases, Adv. Water Resour., 114, 196–218, https://doi.org/10.1016/j.advwatres.2018.02.001,
769 2018.

770 Harp, D. R., Zlotnik, V., Abolt, C. J., Busey, B., Avendaño, S. T., Newman, B. D., Atchley, A. L.,
771 Jafarov, E., Wilson, C. J., and Bennett, K. E.: New insights into the drainage of inundated ice-
772 wedge polygons using fundamental hydrologic principles, The Cryosphere, 15, 4005–4029,
773 https://doi.org/10.5194/tc-15-4005-2021, 2021.

774 Hinzman, L., Busey, B., Cable, W., and Romanovsky, V.: Surface Meteorology, Utqiagvik
775 (Barrow), Alaska, Area A, B, C and D, Ongoing from 2012, 2014.

776 Hjort, J., Karjalainen, O., Aalto, J., Westermann, S., Romanovsky, V. E., Nelson, F. E.,
777 Etzelmüller, B., and Luoto, M.: Degrading permafrost puts Arctic infrastructure at risk by mid-
778 century, Nat. Commun., 9, 5147, https://doi.org/10.1038/s41467-018-07557-4, 2018.

779 Hugelius, G., Strauss, J., Zubrzycki, S., Harden, J. W., Schuur, E. a. G., Ping, C.-L., Schirrmeister,
780 L., Grosse, G., Michaelson, G. J., Koven, C. D., O'Donnell, J. A., Elberling, B., Mishra, U., Camill,
781 P., Yu, Z., Palmtag, J., and Kuhry, P.: Estimated stocks of circumpolar permafrost carbon with
782 quantified uncertainty ranges and identified data gaps, Biogeosciences, 11, 6573–6593,
783 https://doi.org/10.5194/bg-11-6573-2014, 2014.

784 Jafarov, E. E., Coon, E. T., Harp, D. R., Wilson, C. J., Painter, S. L., Atchley, A. L., and
785 Romanovsky, V. E.: Modeling the role of preferential snow accumulation in through talik
786 development and hillslope groundwater flow in a transitional permafrost landscape, Environ. Res.
787 Lett., 13, 105006, https://doi.org/10.1088/1748-9326/aadd30, 2018.

788 Jan, A., Coon, E. T., Painter, S. L., Garimella, R., and Moulton, J. D.: An intermediate-scale model
789 for thermal hydrology in low-relief permafrost-affected landscapes, Comput. Geosci., 22, 163–

790   177, https://doi.org/10.1007/s10596-017-9679-3, 2018.

791   Jan, A., Coon, E. T., and Painter, S. L.: Evaluating integrated surface/subsurface permafrost
792   thermal hydrology models in ATS (v0.88) against observations from a polygonal tundra site,
793   Geosci. Model Dev., 13, 2259–2276, https://doi.org/10.5194/gmd-13-2259-2020, 2020.

794   Jorgenson, M. T., Racine, C. H., Walters, J. C., and Osterkamp, T. E.: Permafrost Degradation and
795   Ecological Changes Associated with a WarmingClimate in Central Alaska, Clim. Change, 48,
796   551–579, https://doi.org/10.1023/A:1005667424292, 2001.

797   Karra, S., Painter, S. L., and Lichtner, P. C.: Three-phase numerical model for subsurface
798   hydrology in permafrost-affected regions (PFLOTRAN-ICE v1.0), The Cryosphere, 8, 1935–1950,
799   https://doi.org/10.5194/tc-8-1935-2014, 2014.

800   Kurylyk, B. L. and Watanabe, K.: The mathematical representation of freezing and thawing
801   processes in variably-saturated, non-deformable soils, Adv. Water Resour., 60, 160–177,
802   https://doi.org/10.1016/j.advwatres.2013.07.016, 2013.

803   Kurylyk, B. L., MacQuarrie, K. T. B., and McKenzie, J. M.: Climate change impacts on
804   groundwater and soil temperatures in cold and temperate regions: Implications, mathematical
805   theory,   and   emerging   simulation   tools,   Earth-Sci.   Rev.,   138,   313–334,
806   https://doi.org/10.1016/j.earscirev.2014.06.006, 2014.

807   Liu, W., Fortier, R., Molson, J., and Lemieux, J.-M.: Three-Dimensional Numerical Modeling of
808   Cryo-Hydrogeological Processes in a River-Talik System in a Continuous Permafrost
809   Environment, Water Resour. Res., 58, e2021WR031630, https://doi.org/10.1029/2021WR031630,
810   2022.

811   Luethi, R., Phillips, M., and Lehning, M.: Estimating Non-Conductive Heat Flow Leading to Intra-
812   Permafrost Talik Formation at the Ritigraben Rock Glacier (Western Swiss Alps), Permafr.
813   Periglac. Process., 28, 183–194, https://doi.org/10.1002/ppp.1911, 2017.

814   McKenzie, J. M. and Voss, C. I.: Permafrost thaw in a nested groundwater-flow system, Hydrogeol.
815   J., 21, 299–316, https://doi.org/10.1007/s10040-012-0942-3, 2013.

816   McKenzie, J. M., Voss, C. I., and Siegel, D. I.: Groundwater flow with energy transport and water–
817   ice phase change: numerical simulations, benchmarks, and application to freezing in peat bogs,
818   Adv. Water Resour., 30, 966–983, https://doi.org/10.1016/j.advwatres.2006.08.008, 2007.

819   NEON (National Ecological Observatory Network): 2D wind speed and direction
820   (DP1.00001.001): RELEASE-2021, 2021.

821   Noh, J.-H., Lee, S.-R., and Park, H.: Prediction of cryo-SWCC during freezing based on pore-size
822   distribution, Int. J. Geomech., 12, 428–438, https://doi.org/10.1061/(ASCE)GM.1943-
823   5622.0000134, 2012.

824   O'Connor, M. T., Cardenas, M. B., Ferencz, S. B., Wu, Y., Neilson, B. T., Chen, J., and Kling, G.
825   W.: Empirical Models for Predicting Water and Heat Flow Properties of Permafrost Soils,

826   Geophys. Res. Lett., 47, e2020GL087646, https://doi.org/10.1029/2020GL087646, 2020.

827   Painter, S. L.: Three-phase numerical model of water migration in partially frozen geological
828   media: model formulation, validation, and applications, Comput. Geosci., 15, 69–85,
829   https://doi.org/10.1007/s10596-010-9197-z, 2011.

830   Painter, S. L. and Karra, S.: Constitutive Model for Unfrozen Water Content in Subfreezing
831   Unsaturated Soils, Vadose Zone J., 13, vzj2013.04.0071, https://doi.org/10.2136/vzj2013.04.0071,
832   2014.

833   Painter, S. L., Coon, E. T., Atchley, A. L., Berndt, M., Garimella, R., Moulton, J. D., Svyatskiy,
834   D., and Wilson, C. J.: Integrated surface/subsurface permafrost thermal hydrology: Model
835   formulation and proof-of-concept simulations: integrated pemafrost thermal hydrology, Water
836   Resour. Res., 52, 6062–6077, https://doi.org/10.1002/2015WR018427, 2016.

837   Ren, J., Vanapalli, S., and Han, Z.: Soil freezing process and different expressions for the soil-
838   freezing characteristic curve, Sci. Cold Arid Reg., 9, 221–228,
839   https://doi.org/10.3724/SP.J.1226.2017.00221, 2017.

840   Riseborough, D., Shiklomanov, N., Etzelmüller, B., Gruber, S., and Marchenko, S.: Recent
841   advances in permafrost modelling, Permafr. Periglac. Process., 19, 137–156,
842   https://doi.org/10.1002/ppp.615, 2008.

843   Rowland, J. C., Travis, B. J., and Wilson, C. J.: The role of advective heat transport in talik
844   development beneath lakes and ponds in discontinuous permafrost, Geophys. Res. Lett., 38,
845   https://doi.org/10.1029/2011GL048497, 2011.

846   Sjöberg, Y., Coon, E., K. Sannel, A. B., Pannetier, R., Harp, D., Frampton, A., Painter, S. L., and
847   Lyon, S. W.: Thermal effects of groundwater flow through subarctic fens: A case study based on
848   field observations and numerical modeling, Water Resour. Res., 52, 1591–1606,
849   https://doi.org/10.1002/2015WR017571, 2016.

850   Stuurop, J. C., van der Zee, S. E. A. T. M., Voss, C. I., and French, H. K.: Simulating water and
851   heat transport with freezing and cryosuction in unsaturated soil: Comparing an empirical, semi-
852   empirical and physically-based approach, Adv. Water Resour., 149, 103846,
853   https://doi.org/10.1016/j.advwatres.2021.103846, 2021.

854   Sugimoto, A., Yanagisawa, N., Naito, D., Fujita, N., and Maximov, T. C.: Importance of
855   permafrost as a source of water for plants in east Siberian taiga, Ecol. Res., 17, 493–503,
856   https://doi.org/10.1046/j.1440-1703.2002.00506.x, 2002.

857   Tesi, T., Muschitiello, F., Smittenberg, R. H., Jakobsson, M., Vonk, J. E., Hill, P., Andersson, A.,
858   Kirchner, N., Noormets, R., Dudarev, O., Semiletov, I., and Gustafsson, Ö.: Massive
859   remobilization of permafrost carbon during post-glacial warming, Nat. Commun., 7, 13653,
860   https://doi.org/10.1038/ncomms13653, 2016.

861   Thornton, M. M., Wei, Y., Thornton, P. E., Shrestha, R., Kao, S., and Wilson, B. E.: Daymet:
862   Station-Level Inputs and Cross-Validation Result for North America, Version 4, 2020.

863 Thornton, P. E., Shrestha, R., Thornton, M., Kao, S.-C., Wei, Y., and Wilson, B. E.: Gridded daily
864 weather data for North America with comprehensive uncertainty quantification, Sci. Data, 8, 190,
865 https://doi.org/10.1038/s41597-021-00973-0, 2021.

866 Van Genuchten, M. T.: A Closed-form Equation for Predicting the Hydraulic Conductivity of
867 Unsaturated Soils, Soil Sci. Soc. Am. J., 44, 892–898,
868 https://doi.org/10.2136/sssaj1980.03615995004400050002x, 1980.

869 Viterbo, P., Beljaars, A., Mahfouf, J.-F., and Teixeira, J.: The representation of soil moisture
870 freezing and its impact on the stable boundary layer, Q. J. R. Meteorol. Soc., 125, 2401–2426,
871 https://doi.org/10.1002/qj.49712555904, 1999.

872 Walvoord, M. A. and Kurylyk, B. L.: Hydrologic Impacts of Thawing Permafrost—A Review,
873 Vadose Zone J., 15, https://doi.org/10.2136/vzj2016.01.0010, 2016.

874 Wasantha Lal, A. M.: Weighted Implicit Finite-Volume Model for Overland Flow, J. Hydraul.
875 Eng., 124, 941–950, https://doi.org/10.1061/(ASCE)0733-9429(1998)124:9(941), 1998.

876 Weismüller, J., Wollschläger, U., Boike, J., Pan, X., Yu, Q., and Roth, K.: Modeling the thermal
877 dynamics of the active layer at two contrasting permafrost sites on Svalbard and on the Tibetan
878 Plateau, The Cryosphere, 5, 741–757, https://doi.org/10.5194/tc-5-741-2011, 2011.

879 Westermann, S., Langer, M., Boike, J., Heikenfeld, M., Peter, M., Etzelmüller, B., and Krinner,
880 G.: Simulating the thermal regime and thaw processes of ice-rich permafrost ground with the land-
881 surface model CryoGrid 3, Geosci. Model Dev., 9, 523–546, https://doi.org/10.5194/gmd-9-523-
882 2016, 2016.

883 Zhang, T., Barry, R. G., Knowles, K., Heginbottom, J. A., and Brown, J.: Statistics and
884 characteristics of permafrost and ground-ice distribution in the Northern Hemisphere, Polar Geogr.,
885 31, 47–68, https://doi.org/10.1080/10889370802175895, 2008.

886